General Disclaimer

One or more of the Following Statements may affect this Document

- This document has been reproduced from the best copy furnished by the organizational source. It is being released in the interest of making available as much information as possible.

- This document may contain data, which exceeds the sheet parameters. It was furnished in this condition by the organizational source and is the best copy available.

- This document may contain tone-on-tone or color graphs, charts and/or pictures, which have been reproduced in black and white.

- This document is paginated as submitted by the original source.

- Portions of this document are not fully legible due to the historical nature of some of the material. However, it is the best reproduction available from the original submission.

Produced by the NASA Center for Aerospace Information (CASI)

NASA CR-144671

(NASA-CR-144671) HONEYCOMB THERMAL SHIELD STUDY Final Report (Wisconsin Univ.) 54 p HC $4.25 CSCL 20M

N75-30480

Unclas

G3/34 34364

SEP 1975
RECEIVED
NASA STI FACILITY
INPUT BRANCH

A REPORT

from the space science and engineering center
the university of wisconsin-madison
madison, wisconsin

Issued 7 February 1975

A Final Report
for the
Honeycomb Thermal Shield Study

Contract Number NAS5-20068

Prepared by

R. M. Dombroski

Space Science and Engineering Center

The University of Wisconsin

for

Goddard Space Flight Center

Greenbelt, Maryland

TABLE OF CONTENTS

		Page
1.0	INTRODUCTION	1
2.0	SUMMARY	2
3.0	ANALYSIS	3
3.1	Isolated Cell Analysis	3
3.2	The Energy Equation for an Isolated Cell	4
3.3	Normalizing of Equations	6
3.4	Energy Equation for a Row of Cells	8
4.0	FINITE ELEMENT MODEL	12
4.1	Single Cell	12
4.2	Cell Row Model	13
5.0	RESULTS AND CONCLUSIONS	14
5.1	Single Cell	14
5.2	Isolated Row of Cells	16
6.0	DESIGN EXAMPLES	19
6.1	Sample Problem Number One, Insulated Shield	19
6.2	Sample Problem Number Two, Conductively Coupled Shield	21
7.0	APPENDICES	24
Appendix A:	Nomenclature	25
Appendix B:	Figures	27
Appendix C:	References	47
Appendix D:	Clear View Calculation	49
Appendix E:	Configuration Factor Calculation	50

1.0 INTRODUCTION

A Honeycomb Thermal Shield is an economical, simple, and reliable alternative to existing thermal shielding methods for reducing the radiated heat loss from elements which will not allow obstructions in the field of view.

The device is simply open-face honeycomb of the type used throughout the aerospace industry for structural panels. The Honeycomb Thermal Shield uses only the core of the honeycomb panel, however, so it has little structural stiffness and is transparent through the cells (see Figure 1). It is located in close proximity to, but conductively decoupled from, the element to be shielded (the radiative source) with the axis of the honeycomb cells parallel to the view direction of the source. The source radiates into a 2π steradian field occupied by the shield. The view field will be transparent along the axis of the honeycomb but will be increasingly obscured as the off-normal view angle increases. The angular dependence is a function of the cell height to width ratio (see Appendix D). A source with a narrow field of view will allow a shield with deep cells (large height to width ratio), and will efficiently trap the radiated energy.

A shielding method which has been used previously required the radiating element to be covered with one or more layers of a low emittance, thin film such as aluminized mylar . For many applications, such as shielding of high energy X-ray detectors, these low emittance films are satisfactory, since the X-rays of interest easily penetrate the film. They are not useful, however, with optical elements or low energy X-ray detectors since they are opaque to the signals of interest.

A development of the energy equations and characteristic system parameters

for the Honeycomb Thermal Shield are found in Section 3. Section 4 describes a finite-difference model for analysis, and Section 5 presents the results of the finite-difference analysis.

2.0 SUMMARY

The Honeycomb Thermal Shield is effective in reducing the radiated energy loss from narrow field-of-view, high sensitivity detectors. For spacecraft applications, the designer may use the shield in one of two modes to achieve the overall system design goals.

The first mode requires the shield be conductively isolated from all sinks. This configuration offers the maximum reduction in heat loss from the system. For a spacecraft application, the terminology might be detector/radiative source, spacecraft/system, space/radative sink. The energy which the shield radiates to space is supplied by the detector, and none is supplied by the spacecraft. The analysis of an isolated single cell describes shield performance in this mode.

The second mode requires the shield to be conductively coupled to the spacecraft. The heat loss from the detector is reduced, but at the expense of increased loss from the spacecraft. The total heat loss to space is greater than would be expected for the isolated shield. Heat transfer in this mode is described in the analysis dealing with an isolated row of cells.

3.0 ANALYSIS

The transfer of energy through a honeycomb shield assembly, Figure 1, comprised of many honeycomb cells with perimeter cells coupled to a thermal sink is a complex process which does not lend itself to either intuitive estimates or closed form analytical solutions.

To reduce the problem to manageable proportions, an analysis will first be developed for a single, isolated, honeycomb cell, Figure 2, then will be expanded to include an isolated row of cells with conductive coupling to a thermal sink, Figures 4 and 5. The single cell analysis is useful in developing the characteristic system parameters and in describing the energy transfer through a conductively isolated shield assembly. The isolated-row model characterizes the performance of a shield which is conductively coupled to a sink.

3.1 Isolated Cell Analysis

Hottel (reference 1) describes the net interchange between equal-area, parallel surfaces, with one a source and one a sink each at a uniform temperature and connected by radiatively adiabatic walls, but neglects axial conduction.

Usiskin and Siegel (reference 2) characterize the transfer of energy through a cylindrical enclosure with a specified wall heat flux, but again axial conduction through the enclosure wall is neglected. In fact, none of the treatments listed in the references specifically address the transfer through honeycomb elements.

The energy equation for a single isolated cell provides a simplified

mathematical model which can be normalized to yield the dimensionless system parameters. The single cell has design significance as well as mathematical significance since shield performance for several situations can be described by this simple system. The model can be used, for instance, for conductively isolated shields having negligible lateral thermal gradients compared with the axial (through the cell) gradient. It is also applicable to the design of very large shields which are conductively coupled to a sink, but whose innermost cells are receiving no laterally conducted energy. These applications are discussed in detail in section 6.

A schematic representation of a honeycomb cell is shown in Figure 2. Surfaces A_1 and A_2 are isothermal, diffuse, black sinks, and it is the net radiative energy transfer between these sinks which is of importance to this analysis.

The interior surface of the honeycomb cell is diffuse and gray, and the exterior is insulated.

Energy transfer is by conduction through the cell wall and by radiation between all elements within the enclosure.

All specified properties are assumed constant, and the system is operating at steady state.

3.2 The Energy Equation for an Isolated Cell

The following analysis parallels related presentations in references 2 and 5. Terms appearing in the following equations are defined in Appendix A.

The transfer of energy through a typical element, dA_i, of the isolated cell is described by the equation:

$$dQ_{rad})_{net} + dQ_{cond})_{net} = 0 \qquad \text{EQ 1}$$

where: $dQ_{rad})_{net}$ is the net energy into the element by radiation

$dQ_{cond})_{net}$ is the net energy into the element by conduction

Since gradients in the x-direction are assumed small, the conduction term accounts only for transfer in the y-direction.

Expanding the conduction term:

$$dQ_{cond})_{net} = dQ_{cond})_y = \frac{d}{dy}\left[-ktdx\frac{dT(y)}{dy}\right]dy \qquad \text{EQ 2}$$

$$dA_i = (dx)(dy) \qquad \text{EQ 3}$$

$$dQ_{cond})_y = -kt\,\frac{d^2T(y)}{dy^2}\,dA_i \qquad \text{EQ 4}$$

A similar expansion of the radiation term yields:

$$dQ_{rad})_{net} = [B(y) - H(y)]\,dA_i \qquad \text{EQ 5}$$

where: $B(y) = \varepsilon\sigma T^4(y) - \rho H(y)$ EQ 6

$\rho = 1 - \varepsilon$ EQ 7

$$H(y) = \sigma T_1^4 F_{y-1} + \sigma T_2^4 F_{y-2} + \int_o^{y/a} \varepsilon\sigma T^4\left(\frac{\eta'}{a}\right)K\left(\frac{y-\eta'}{a}\right)d\left(\frac{\eta'}{a}\right) + \int_{(y/a)}^{(H/a)} \varepsilon\sigma T^4\left(\frac{\eta'}{a}\right)K\left(\frac{\eta'-y}{a}\right)d\left(\frac{\eta'}{a}\right) \qquad \text{EQ 8}$$

and: F_{y-1} is the configuration factor between element A_i and area A_1

F_{y-2} is the configuration factor between element A_i and area A_2

$K(\frac{y-\eta'}{a})$ is the configuration factor between element A_i and element A_j for $\eta' < y$

$K(\frac{\eta'-y}{a})$ is the configuration factor between element A_i and element A_j for $\eta' > y$.

The boundary conditions are:

$$\frac{dT(y)}{dy} = 0 \qquad \text{at } y = 0$$

$$\frac{dT(y)}{dy} = 0 \qquad \text{at } y = H$$

The above integro-differential equation can be solved by numerical techniques. First, however, the equations will be normalized to determine the characteristic dimensionless parameters, then a finite difference model will be developed.

3.3 Normalizing of Equations

Performing a strict normalization of the equations for a honeycomb cell is tedious because of the complex nature of the configuration factor kernel terms. The normalization of equations for a cylinder, Figure 3, is less complex, but yields the same dimensionless groups. Therefore in the normalization below, the H(y) terms are correct only for a cylinder, but the resultant dimensionless groups are correct for a honeycomb cell also.

The angle factors F and K have been presented in reference 2 as:

$$F_{y-1} = \frac{(\frac{y}{a})^2 + (\frac{1}{2})}{\{(\frac{y}{a})^2 + 1\}^{1/2}} - (\frac{y}{a}) \qquad \text{EQ 9}$$

$$F_{y-2} = \frac{(\frac{H-y}{a})^2 + (\frac{1}{2})}{\{(\frac{H-y}{a})^2 + 1\}^{1/2}} - (\frac{H-y}{a}) \qquad \text{EQ 10}$$

$$K(\frac{y-\eta'}{a}) = 1 - \frac{|(\frac{y-\eta'}{a})^3| - \frac{3}{2}|(\frac{y-\eta'}{a})|}{\{(\frac{y-\eta'}{a})^2 + 1\}^{3/2}} \qquad \text{EQ 11}$$

$$K(\frac{\eta'-y}{a}) = 1 - \frac{|(\frac{\eta'-y}{a})^3| - \frac{3}{2}|(\frac{\eta'-y}{a})|}{\{(\frac{\eta'-y}{a})^2 + 1\}^{3/2}} \qquad \text{EQ 12}$$

Defining the normalization variables as:

$$\theta_y = \frac{T(y)}{T_1} ; \quad \theta_\eta = \frac{T(\frac{\eta'}{a})}{T_1} ; \quad Y = \frac{y}{H} ; \quad \eta = \frac{\eta'}{H} ; \quad \beta(Y) = \frac{B(y)}{\sigma T_1^{\,4}} ;$$

$$\Psi(Y) = \frac{H(y)}{\sigma T_1^{\,4}}$$

and summing equations 1 through 12:

$$\frac{d^2\theta_y}{dY^2} = \left[\frac{H^2\sigma T_1^{\,3}}{kt}\right][\beta(Y) - \Psi(Y)] \qquad \text{EQ 13}$$

$$\beta(Y) = \varepsilon\theta_y^{\,4} - \rho\Psi(Y) \qquad \text{EQ 14}$$

$$\Psi(Y) = \left[\frac{(\frac{H}{a})^2 Y^2 + (\frac{1}{2})}{\{(\frac{H}{a})^2 Y^2 + 1\}^{1/2}} - (\frac{H}{a})Y\right] + (\frac{T_2}{T_1})^4\left[\frac{(\frac{H}{a})^2(1 - Y)^2 + (\frac{1}{2})}{\{(\frac{H}{a})^2(1-Y)^2 + 1\}^{1/2}} - (\frac{H}{a})(1 - Y)\right]$$

$$+ \varepsilon\int_0^{(\frac{H}{a})Y} \theta_\eta^4 K(\frac{y-\eta'}{a})(\frac{H}{a})d\eta + \varepsilon\int_{(\frac{H}{a})Y}^{1} \theta_\eta^4 K(\frac{\eta'-y}{a})(\frac{H}{a})d\eta \qquad \text{EQ 15}$$

$$K(\frac{y-\eta'}{a}) = 1 - \frac{|(\frac{H}{a})^3(Y-\eta)^3| + \frac{3}{2}|(\frac{H}{a})(Y-\eta)|}{\{(\frac{H}{a})^2(Y-\eta)^2 + 1\}^{3/2}} \qquad \text{EQ 16}$$

$$K(\frac{\eta'-y}{a}) = 1 - \frac{|(\frac{H}{a})^3(\eta-Y)^3| + \frac{3}{2}|(\frac{H}{a})(\eta-Y)|}{\{(\frac{H}{a})^2(\eta-Y)^2 + 1\}^{3/2}} \qquad \text{EQ 17}$$

The normalized boundary conditions are:

$$\frac{d\theta_y}{dY} = 0 \quad \text{at } Y = 0$$

$$\frac{d\theta_y}{dY} = 0 \quad \text{at } Y = 1$$

Inspection of equations 13 through 17 identifies four dimensionless parameters:

1) ε

2) $(\frac{T_2}{T_1})$

3) $(\frac{H}{a})$

4) $[\frac{H^2\sigma T_1^{\ 3}}{kt}]$

The first three of these might have been selected on intuition, but the meaning of the fourth might be less obvious. Defining the conductive and radiative transfer at element A_i with unit emissivity as:

$$Q_{cond} = \frac{k(t\Delta x)(T_i - T_j)}{\Delta y}$$

$$Q_{rad} = \sigma(\Delta x \cdot \Delta y)(T_i^{\ 4} - T_j^{\ 4}) \approx \sigma(\Delta x \cdot \Delta y)[4T_i^{\ 3}(T_i - T_j)] \ *$$

and taking the ratio:

$$\frac{Q_{rad}}{Q_{cond}} = \frac{4\sigma(\Delta x \cdot \Delta y)T_i^{\ 3}(T_i - T_j)\Delta y}{kt\Delta x(T_i - T_j)} \quad \text{, then}$$

$$\frac{Q_{rad}}{Q_{cond}} = \frac{4\sigma\Delta y^2 T_i^{\ 3}}{kt}$$

Since H is the characteristic dimension in the y-direction, this may be reexpressed as

$$\boxed{(\frac{1}{4})\frac{Q_{rad}}{Q_{cond}} = N_c = \frac{H^2\sigma T^3}{kt}}$$

The term N_c will hereinafter be referred to as the thermal coupling parameter.

3.4 Energy Equation for a Row of Cells

Lateral as well as axial conduction must be accounted for in the energy equation for a row of cells since the first cell in the row is

*A binomial expansion of $(1 - \frac{\Delta T}{T_i})^4$

conductively coupled to a sink at temperature T_o. Referring to Figure 4, conduction in the z-direction is assumed small as is the conduction from the last cell of the row. This is a reasonable assumption if the row element under consideration is in a field having a weak gradient across each cell (see Figure 6).

The energy equation for an element A_i is:

$$dQ_{cond})_{net} + dQ_{rad})_{net} = 0 \qquad \text{EQ 18}$$

Expanding the conduction term:

$$dQ_{cond})_{net} = \frac{d}{dx}[-ktdy\frac{dT(x)}{dx}]dx + \frac{d}{dy}[-ktdx\frac{dT(y)}{dy}]dy \qquad \text{EQ 19}$$

$$dA_i = dx \cdot dy \qquad \text{EQ 20}$$

Similarly for the radiation term:

$$dQ_{rad})_{net} = [B(x,y) - H(x,y)]dA_i \qquad \text{EQ 21}$$

Making a further assumption that gradients within any one cell are small in the x-direction for purposes of calculating the radiative coupling, Equation 21 for a cell row will be identical to the development of Equation 5 for an isolated cell.

The boundary conditions are:

$$T(x) = T_o \text{ at } x=0; \ \frac{dT(x)}{dx} = 0 \text{ at } x=s; \ \frac{dT(y)}{dy} = 0 \text{ at } y=0; \ \frac{dT(y)}{dy} = 0 \text{ at } y=H.$$

Normalizing variables are:

$$\theta_x = \frac{T(x)}{T_o}; \quad \theta_y = \frac{T(y)}{T_o}; \quad \theta_\eta = \frac{T(\eta'/a)}{T_o}; \quad X = \frac{x}{a}; \quad Y = \frac{y}{H}; \quad \eta = \frac{\eta'}{H};$$

$$\beta(Y) = \frac{B(y)}{\sigma T_1^4}; \quad \Psi(Y) = \frac{H(y)}{\sigma T_1^4}.$$

Substituting into equations 18 through 21:

$$(\frac{H}{a})^2\frac{d^2\theta_x}{dX^2} + \frac{d^2\theta_y}{dY^2} = (\frac{T_1}{T_o})[\frac{H^2\sigma T_1^3}{kt}][\beta(Y) - \Psi(Y)] \qquad \text{EQ 22}$$

$$\beta(Y) = \varepsilon\theta_y^{\,4} - \rho\Psi(Y) \qquad \text{EQ 23}$$

$$\Psi(Y) = \left[\frac{(\frac{H}{a})^2 Y^2 + (\frac{1}{2})}{\{(\frac{H}{a})^2 Y^2 + 1\}^{1/2}} - (\frac{H}{a})Y\right] + (\frac{T_2}{T_1})^4 \left[\frac{(\frac{H}{a})^2 (1 - Y)^2 + (\frac{1}{2})}{\{(\frac{H}{a})^2 (1 - Y)^2 + 1\}^{1/2}} - (\frac{H}{a})(1 - Y)\right]$$

$$+ \varepsilon(\frac{T_o}{T_1})^4 \int_o^{(\frac{H}{a})Y} \theta_\eta^{\,4} K(\frac{y - \eta'}{a})(\frac{H}{a})d\eta + \varepsilon(\frac{T_o}{T_1})^4 \int_{(\frac{H}{a})Y}^{1} \theta_\eta^{\,4} K(\frac{\eta' - y}{a})(\frac{H}{a})d\eta \qquad \text{EQ 24}$$

$$K(\frac{y - \eta'}{a}) = 1 - \frac{|(\frac{H}{a})^3 (Y - \eta)^3| + \frac{3}{2}|(\frac{H}{a})(Y - \eta)|}{\{(\frac{H}{a})^2 (Y - \eta)^2 + 1\}^{3/2}} \qquad \text{EQ 25}$$

$$K(\frac{\eta' - y}{a}) = 1 - \frac{|(\frac{H}{a})^3 (\eta - Y)^3| + \frac{3}{2}|(\frac{H}{a})(\eta - Y)|}{\{(\frac{H}{a})^2 (\eta - Y)^2 + 1\}^{3/2}} \qquad \text{EQ 26}$$

with boundary equations:

$\theta_x = 1$ at $X=0$; $\frac{d\theta_x}{dX} = 0$ at $X = (\frac{s}{a})$; $\frac{d\theta_y}{dY} = 0$ at $y=0$; $\frac{d\theta_y}{dY} = 0$ at $y=0$.

The resultant dimensionless parameters are:

1) ε

2) $(\frac{T_2}{T_1})$

3) $(\frac{H}{a})$

4) $[\frac{H^2\sigma T_1^{\,3}}{kt}]$

5) $(\frac{T_o}{T_1})$

6) $(\frac{s}{a})$

The first four parameters are identical to those developed for the isolated cell. The temperature ratio (T_o/T_1) accounts for the conductive boundary condition, and (s/a) is proportional to the number of cells in the cell row.

4.0 FINITE ELEMENT MODEL

4.1 Single Cell

The finite element model for a single cell is shown in Figure 7. The enclosure has six nodes: four are elements of a honeycomb cell and the remaining two the radiative sink and source. Axial conductance between nodes three through six is:

$$C_a = \frac{1}{R_a} = \frac{(k)(6at)}{(H/4)}$$

Honeycomb node area is:

$$A = \frac{6aH}{4}$$

and source area $A_1 = A_2 = W^2 \sin 60°$.

Nineteen radiation configuration factors (F) are required to describe the transfer between the six nodes. Feingold (Reference 3) determined the factor F_{12} for honeycomb cells for thirty-two different values of (a/H) from 0.05 to 20.0. Using these values and configuration factor algebra, it is possible to calculate all interchange factors. The tabulated values from Feingold are included in Appendix D along with the algebraic equations used to calculate all of the F-factor terms. For those values of (a/H) not tabulated, the analysis relied on a linear interpolation between adjacent points. Further, the analysis was restricted to those values between 0.05 and 20.0.

A finite difference computer program, developed at the University of Wisconsin, allows the user to provide two subroutines, one for inputting and/or calculating data to be read in, and one for calculating and/or formatting output data which might not be included in the standard program format. The following system parameters are read in along with Table D1:

1) W
2) H
3) k
4) t
5) ε
6) T_1
7) T_2

All other required parameters such as estimated temperatures for nodes 3 through 6, areas, configuration factors, and conductive couplings are calculated within the program.

4.2 Cell Row Model

The model for a cell row is illustrated in Figure 8. A significant increase in the number of nodes and interchange coupling factors is now possible. For instance, a 15 cell model has 91 nodes, 285 radiation interchange factors, and 136 conduction interchange factors. The factors R_A and A are as defined for the single cell. The lateral conductance is:

$$R_1 = \frac{(k)(\frac{H}{4})(t)(2)}{4a}$$

for cell rows as shown in Figure 5, and

$$R_2 = \frac{(k)(\frac{H}{4})(t)(2)}{2a} = 2R_1$$

for cell rows as shown in Figure 4.

The following system parameters are read in along with Table D1:

1) W
2) H
3) k
4) t
5) ε
6) N (number of honeycomb cells)
7) T_o
8) T_2
9) T_1

From these, all other required parameters are calculated within INPUT.

5.0 RESULTS AND CONCLUSIONS

5.1 Single Cell

Figures 9 and 10 illustrate the variation of shielding efficiency, η, as a function of the cell parameters L and N_c. The efficiency is defined such that as the net energy transfer from A_1 to A_2 decreases, η increases.

Several general characteristics can be observed following a cursory examination of the graphs. First of all, η is relatively independent of N_c for L less than 2. Also, the variation of η is small in all cases for N_c greater than 50.

A significant finding not graphically illustrated is that η is independent of the fourth power temperature difference:

$$(T_1^4 - T_2^4) = T_1^4[1 - (\frac{T_2}{T_1})^4]$$

Dependence might have been expected since the temperature ratio (T_2/T_1) appeared as a characteristic dimensionless parameter in the energy equation. A possible physical interpretation of this result is that the honeycomb reduces the emissivity of the radiating source, and that the effective emissivity, ε_{eff}, is independent of the environment:

$$\varepsilon_{eff} = 1 - \eta \neq f(\frac{T_2}{T_1})$$

Higher efficiencies resulting from strong axial gradients are noted for L greater than 2 and for increasing N_c. For cells of low axial thermal conductance (large N_c), the radiated energy from A_1 is absorbed predominantly at the base of the cell (T_{base}) and is reradiated at a lower temperature (T_{top}). It is the absorption at T_{base} and reradiation at

$T_{top} < T_{base}$ which increases the shielding efficiency from 0.5 to 0.72 for $L = 8$ and $\varepsilon = 1$.

The intersection of all efficiency curves with the vertical axis can be predicted by simply using the three-body radiation equation. The third surface, the honeycomb cell, is insulated, isothermal, reradiating and black. The energy equation is:

$$Q_{rad_2} = \frac{\sigma A_1 (T_1^4 - T_2^4)}{\frac{A_1 + A_2 - 2A_1F_{12}}{A_2 - A_1(F_{12})^2} + (\frac{1}{\varepsilon_1} - 1) + \frac{A_1}{A_2}(\frac{1}{\varepsilon_2} - 1)}$$

For $\varepsilon_1 = \varepsilon_2 = 1$; $A_1 = A_2$ and $\eta = 1 - \frac{Q_{rad_2}}{\sigma A_1 (T_1^4 - T_2^4)}$, this can be reexpressed as:

$$\eta = \frac{1}{2}(1 - F_{12}) \qquad \text{EQ 27}$$

The values of F_{12} of Table D1 and Equation 27 will predict the shielding efficiency for any black, high-conductance honeycomb shield.

Hottel (Reference 1, Section 3.12) presents a method for estimating η for cylinders which can be used with reasonable judgment to predict η for honeycomb cells of large N_c. Figure 11 is reproduced from Hottel for reference purposes $[\eta = 1 - \overline{(s_1, s_2)}_R]$.

It is possible to predict the effect of adding one non-conducting shield to a second non-conducting shield with the simple two body radiation equation.

$$Q_{rad_2} = \frac{\sigma (T_1^4 - T_2^4)}{[\frac{1 - \varepsilon_1}{\varepsilon_1 A_1} + \frac{1 - \varepsilon_2}{\varepsilon_2 A_2} + \frac{1}{A_1 F_{12}}]}$$

For $A_1 = A_2$, $F_{12} = 1$, $\varepsilon_1 = 1 - \eta_1$, and $\varepsilon_2 = 1 - \eta_2$, this equation reduces to:

$$\frac{Q_{rad_2}}{\sigma A_1 (T_1^4 - T_2^4)} = 1 - \eta_{eff} = \frac{1}{[\frac{\eta_1}{1 - \eta_1} + \frac{\eta_2}{1 - \eta_2} + 1]}$$

Rearranging:

$$\eta_{eff} = 1 - \frac{1}{\left[\frac{\eta_1}{1 - \eta_1} + \frac{\eta_2}{1 - \eta_2} + 1\right]} \qquad \text{EQ 28}$$

For example, to find the effective efficiency, η_{eff}, for a two shield stack each with L = 4 and N_c = 100, it is necessary to know only the efficiency of each shield:

$$\eta_1 = \eta_2 = 0.636$$

$$\eta_{eff} = 1 - \frac{1}{\frac{0.636}{1 - 0.636} + \frac{0.636}{1 - 0.636} + 1}$$

$$\boxed{\eta_{eff} = 0.778}$$

This result is within 7% of the predicted value for L = 8. It is possible to predict the efficiency for any value of L between 0.5 and 8 and for large N_c to an estimated accuracy of better than 10%.

A comparison of Figures 9 and 10 indicates that decreasing the bulk surface emissivity of the honeycomb has a significant impact on η only for small N_c and large L.

5.2 Isolated Row of Cells

The results for an isolated row of cells are illustrated in Figures 12 through 18.

The efficiency must be considered from two different points of view for cell rows. First of all there is the apparent shielding efficiency as viewed from surface A_1 (the source):

$$\eta_1 = 1 - \frac{Q_{rad_1}}{\sigma A_1 T_1^4} \qquad \text{EQ 29}$$

As the energy loss from surface 1 decreases, the efficiency increases. Second is the apparent radiating efficiency as viewed from A_2 (the sink):

$$\eta_2 = 1 - \frac{Q_{rad_2}}{\sigma A_1 T_1^4} \qquad \text{EQ 30}$$

Again, as the transfer to surface 2 decreases, the efficiency increases.

For the single isolated cell, η_1 is identically equal to η_2, but this is not true for the cell row since energy is conductively added:

$$Q_{rad_2} = Q_{rad_1} + Q_{cond}$$

where: Q_{cond} is the energy conducted from the mounting surface at T_o.

$$Q_{cond} = Q_{rad_2} - Q_{rad_1} \qquad \text{EQ 31}$$

Combining Equations 29, 30, and 31:

$$Q_{cond} = Q_{sink} = \sigma A_1 T_1^4 (\eta_1 - \eta_2)$$

$$\frac{Q_{sink}}{\sigma A_1 T_1^4} = \eta_1 - \eta_2$$

Clearly, as η_1 approaches η_2 the cell response approaches that of an isolated cell.

It must be pointed out that a <u>low</u> radiating efficiency (η_2) may be a design goal. If, for instance, the goal is to minimize the energy loss from the source (A_1) trading off a larger heat loss from the conductive sink, then a conductively coupled shield of low N_c and η_2 is desirable.

Figures 12 and 13 show, as expected, a strong variation of η with distance from the conductive sink for the specified cell parameters. A highly conductive shield with a small number of cells of large L radiates as a blackbody at T_o. As more and more cells are added, the influence of

lateral conductance decreases, and the innermost cells perform closely as an isolated cell. The lateral conductance for the situation illustrated in Figure 4 is two times as large as that for Figure 5, and the corresponding decrease in efficiency is apparent. Note the slope is near zero for the last cell for all situations due to the imposed boundary condition on that cell.

Figures 14 and 15 show again the variation of η, but this time for an L of 4. The results for 5 and 10 cells coincide with the 15 cell graph (i.e. one graph can be used for any number of cells). For L less than 4, there is very weak dependence of η on cell position, and an isolated cell assumption is reasonable for all cells of the row.

Figures 16 and 17 illustrate the variation of efficiency as a function of number of cells and N_c for $(T_o/T_1) = 1$ and $\varepsilon = 1$.

Finally Figure 18 shows the efficiency trend for various ratios (T_1/T_o). For all cases, $T_1 = 298.15°K$.

6.0 DESIGN EXAMPLES

Two sample problems will illustrate the usefulness of the graphs for an application having two different design goals.

6.1 Sample Problem Number One

Assume a sensitive detector with a large aperture is to be launched as part of a small satellite. The goal is to reduce both the total heat loss from the spacecraft and to minimize the heat loss from the detector. Based on a determination of the input signal attenuation (reduction of field of view) due to shielding, the cell L-ratio must be 4 or less. The detector temperature is to be maintained at 25°C and its black aperture will be continuously directed toward deep space.

To reduce both total energy loss and detector loss, the shield must be thermally isolated from the spacecraft. This will allow the shield to become as cold as possible, thus radiating the minimum energy. In addition the N_c value should be maximized to take advantage of axial cell gradients.

Making a preliminary selection of a 1/2 inch deep by 1/4 inch wide aluminum cell with 0.0007 inch wall thickness:

H = 0.5; W = .25; k = 90 BTU/(hrft °F); t = 0.0007 inch; and L = 3.5

$$N_c = \frac{H^2 \sigma T_1^{\,3}}{ktc} = \frac{(0.5)^2(5.67 \times 10^{-12})(298.15)^3}{(90)(0.0007)(0.68 \times 10^{-2})}$$

where c is a conversion factor making the ratio dimensionless

$$\boxed{N_c = 0.09}$$

The efficiency, η, for a black shield is 0.5 as noted on Figure 9, and for ε = .6 from Figure 10 is 0.54. Using η = 0.5:

$$\frac{Q_{rad_1}}{A_1} = \frac{Q_{rad_2}}{A_1} = (1 - \eta)[\sigma(T_1^{\,4} - T_2^{\,4})]$$

$$\frac{Q_{rad_2}}{A_1} = (0.5)(5.67 \times 10^{-12})(298.15)^4$$

$$\boxed{\frac{Q_{rad_1}}{A_1} = 2.2 \times 10^{-2} \text{ watts/cm}^2}$$

or:

$$\frac{Q_{rad_1}}{\text{cell}} = \frac{Q_{rad_1}}{A_1} = \frac{2.2 \times 10^{-2}}{W^2 \sin 60°}$$

$$\boxed{\frac{Q_{rad_1}}{\text{cell}} = 6.3 \times 10^{-2} \text{ watts/cell}}$$

It is now simply a matter of counting the number of cells in the shield and multiplying by 0.0632 watts/cell.

Had a plasticized-paper honeycomb been selected with:

$H = 0.5$ inch; $W = 0.25$ inch; $t = .005$ inch; $k = 0.1$ BTU/hr ft °F; then

$L = 3.5$; $N_c = 11$; and $\eta \approx .54$ for $\varepsilon = 1.0$; $\eta \approx .58$ for $\varepsilon = 0.6$.

A relatively small improvement over the aluminum shield. However, by changing the cell selection slightly to:

$H = 1.0$ inch; $W = 0.5$ inch; $t = 0.005$ inch; $k = 0.1$ BTU/hr ft °F; then

$L = 3.5$; $N_c = 44$; and $\eta \approx 0.64$ for $0.6 \leq \varepsilon \leq 1$. The cell energy loss is then:

$$\frac{Q_{rad_1}}{A_1} = 1.6 \times 10^{-2} \text{ watts/cm}^2$$

$$\frac{Q_{rad_1}}{\text{cell}} = 1.1 \times 10^{-2} \text{ watts/cell}$$

The three cases considered are summarized below:

CASE	DESCRIPTION	EFFICIENCY	
		$\varepsilon = 1.0$	$\varepsilon = 0.6$
1	Aluminum honeycomb, 1/2 x 1/4 cells	0.50	0.54
2	Plasticized paper honeycomb, 1/2 x 1/4 cells	0.54	0.58
3	Plasticized paper honeycomb, 1 x 1/2 cells	0.64	0.64

6.2 Sample Problem Number Two

Assume again a sensitive detector with a large aperture is to be launched as part of a spacecraft and the detector requires thermal shielding. The design goal is to minimize the heat loss from the detector. Conducted thermal energy of less than 15 watts may be drawn from the spacecraft and reradiated from the shield to space. The detector aperture is a square, twelve inches on a side. The cell aspect ratio (L) must be 8 or less. Both the detector and spacecraft frame are expected to operate at 25°C.

To illustrate the method, assume $N_c = 1$ for a 1.125 inch high by 0.25 inch width cell having $\varepsilon = 1$.

Then: $H = 1.125$; $W = 0.25$; $L = 7.8$; $N_c = 1.0$; $\varepsilon = 1.0$; $(T_o/T_1) = 1.0$.

Referring to design graphs 12 and 13, at a distance of 15 cells from the sink at T_o the efficiency is closely that of an isolated cell.

Lines of equal efficiency (similar to isotherms) are plotted in Figure 19. Keep in mind the number of cells per inch is:

$$\text{high conductance direction (cells/inch)} = \frac{1}{W} = \frac{1}{.25} = 4$$

$$\text{low conductance direction (cells/inch)} = \frac{1}{1.73\,W} = \frac{1}{(1.73)(.25)} = 2.31$$

The total shield area is 144 square inches and the cell area is 0.054 square inches.

The area within the inner ellipse of Figure 19 is radiating as an

isolated cell of $\eta_1 = \eta_2 = 0.50$. For larger ellipses, assume a linear interpolation between "isotherm" values (This obviously can be improved by weighting the difference closer to the lower values of η_2).

If we designate the area of the inner ellipse as A_{E0} and the area between each succeeding ellipse as A_{E1}, A_{E2}, etc.:

$$A_{E0} = \frac{\pi}{4} (\ell_o \, h_o)$$

ℓ_o = minor diameter

h_o = major diameter

$$A_{E0} = \frac{\pi}{4} (4.5) \; (4.5)$$

$A_{E0} = 15.9 \text{ in}^2$	$\eta_2)_0 = 0.50$	$\eta_1)_0 = .50$
$A_{E1} = 20.0 \text{ in}^2$	$\eta_2)_1 = 0.44$	$\eta_1)_1 = .57$
$A_{E2} = 26.2 \text{ in}^2$	$\eta_2)_2 = 0.37$	$\eta_1)_2 = .61$
$A_{E3} = 24.1 \text{ in}^2$	$\eta_2)_3 = 0.29$	$\eta_1)_3 = .71$
$A_{E4} = 47.8 \text{ in}^2$	$\eta_2)_4 = 0.12$	$\eta_1)_4 = .79$
$A_{TOT} = 144.0 \text{ in}^2$		

$$\eta_2)_{TOT} = \frac{1}{A_{TOT}} [A_{E0}\eta_2)_0 + A_{E1}\eta_2)_1 + A_{E2}\eta_2)_2 + A_{E3}\eta_2)_3 + A_{E4}\eta_2)_4]$$

$$\boxed{\eta_2)_{TOT} = 0.30}$$

Similarly:

$$\boxed{\eta_1)_{TOT} = 0.64}$$

The average shielding efficiencies can then be used to compute the heat loss terms.

$$\frac{Q_{sink}}{\sigma \ell_1 T_1^4} = \eta_1 - \eta_2 = 0.64 - 0.30 = 0.34$$

$$Q_{sink} = (0.34)(5.67 \times 10^{-12})(144)(2.54)^2(298.15)^4$$

$$Q_{sink} = (0.34)(41.63)$$

$$\boxed{Q_{sink} = 14.15 \text{ watts}}$$

$$Q_{rad_2} = \sigma A_1 T_1^4(1 - \eta_2) = \sigma A_1 T_1^4(1 - 0.3)$$

$$\boxed{Q_{rad_2} = 29.14 \text{ watts}}$$

$$Q_{rad_1} = \sigma A_1 T_1^4(1 - \eta_1) = \sigma A_1 T_1^4(1 - .64)$$

$$\boxed{Q_{rad_1} = 14.99 \text{ watts}}$$

Summarizing:

1) Loss with no shield = 41.63 watts

2) Loss from shielded detector = 14.99 watts

   Loss from spacecraft = 14.15 watts

   Total loss to space = 29.14 watts

7.0 APPENDICES

Appendix A: Nomenclature

Appendix B: Figures

Appendix C: References

Appendix D: Clear View Calculation

Appendix E: Configuration Factor Calculation

APPENDIX A

NOMENCLATURE

a	honeycomb dimension per Figure 2; also cylinder diameter per Figure 3
A	honeycomb node area in finite difference model
A_i	area of element i for radiation
A_1	radiative source area of honeycomb or cylinder
A_2	radiative sink area of honeycomb or cylinder
$B(y)$	combined radiative flux (emitted plus reflected) leaving surface A_i at location y
F	configuration factor
H	honeycomb cell height; also cylinder height
$H(y)$	incident radiative flux on surface A_i
k	thermal conductivity of honeycomb wall
L	ratio of H/a
N	number of cells in an isolated row
N_c	thermal coupling parameter $[\frac{H^2 \sigma T_1^3}{kt}]$
Q_{cond}	heat transferred by conduction
Q_{rad_1}	also QRAD(1); net heat transfer from A_1
Q_{rad_2}	also QRAD(2); net heat transfer from A_2
Q_{sink}	net heat transfer from sink at T_o
R_a	axial conductive resistance between honeycomb nodes
R_L	lateral conductive resistance between honeycomb nodes
R_1	R_L for low conductance cell direction
R_2	R_L for high conductance cell direction
s	length of cell row
t	honeycomb cell wall thickness
T_o	temperature of conductive sink
T_1	temperature of radiative source

T_2	temperature of radiative sink
$T(x)$	honeycomb temperature at location x
$T(y)$	honeycomb temperature at location y
W	honeycomb width across flats
x	dimension along coordinate x
X	dimensionless coordinate, x/a
y	dimension along coordinate y, y/H
Y	dimensionless coordinate
ε	surface emissivity
ρ	surface reflectivity = $1 - \varepsilon$
σ	Stefan-Boltzman constant
η	shielding efficiency; also dimensionless dummy integration variable in energy equation (η'/H)
η'	dummy integration variable
θ_x	dimensionless temperature at coordinate X
θ_y	dimensionless temperature at coordinate Y
θ_η	dimensionless temperature at coordinate $\eta H/a$
$\beta(Y)$	dimensionless flux $B(y)/\sigma T_1^4$
$\Psi(Y)$	dimensionless flux $H(y)/\sigma T_1^4$

APPENDIX B

FIGURES

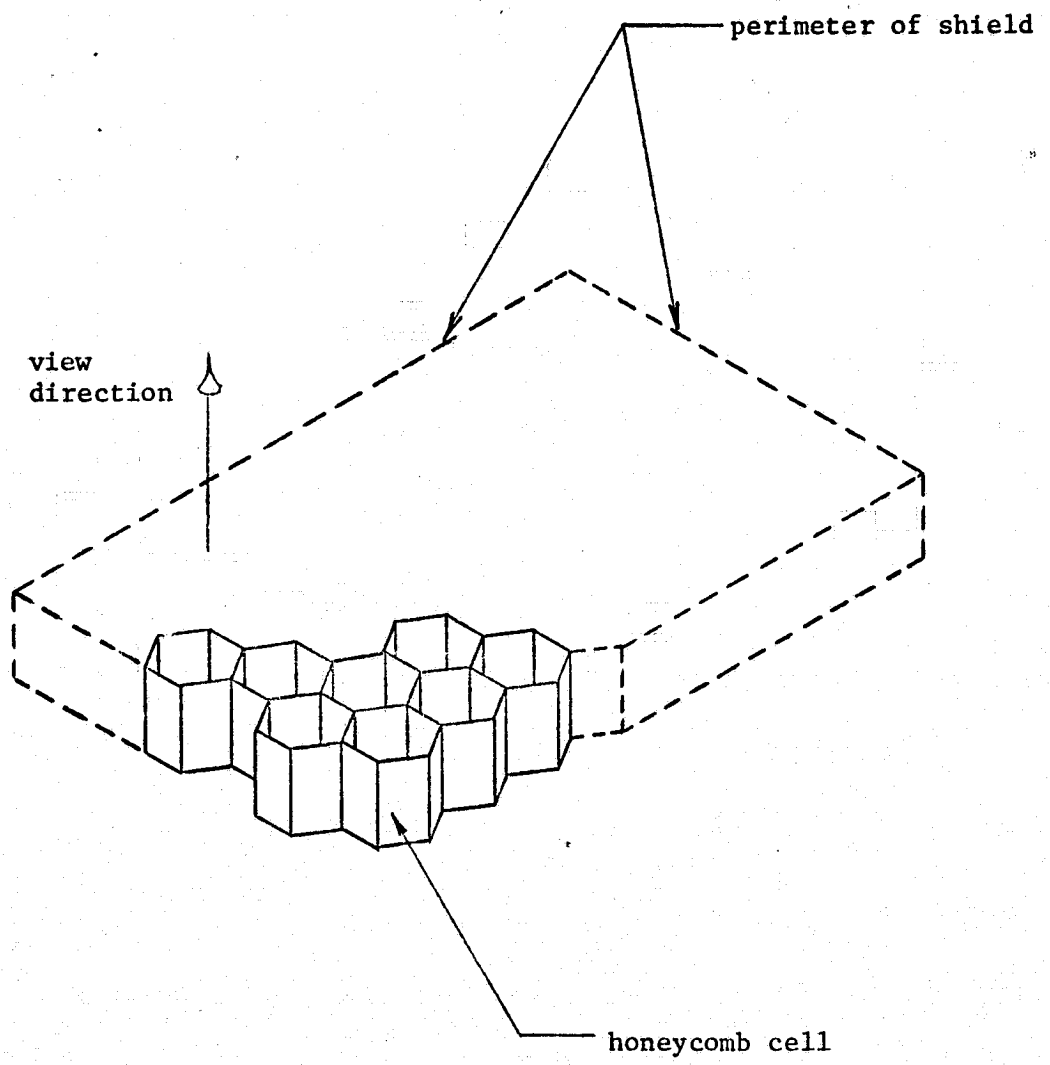

Figure 1. Honeycomb Thermal Shield Schematic

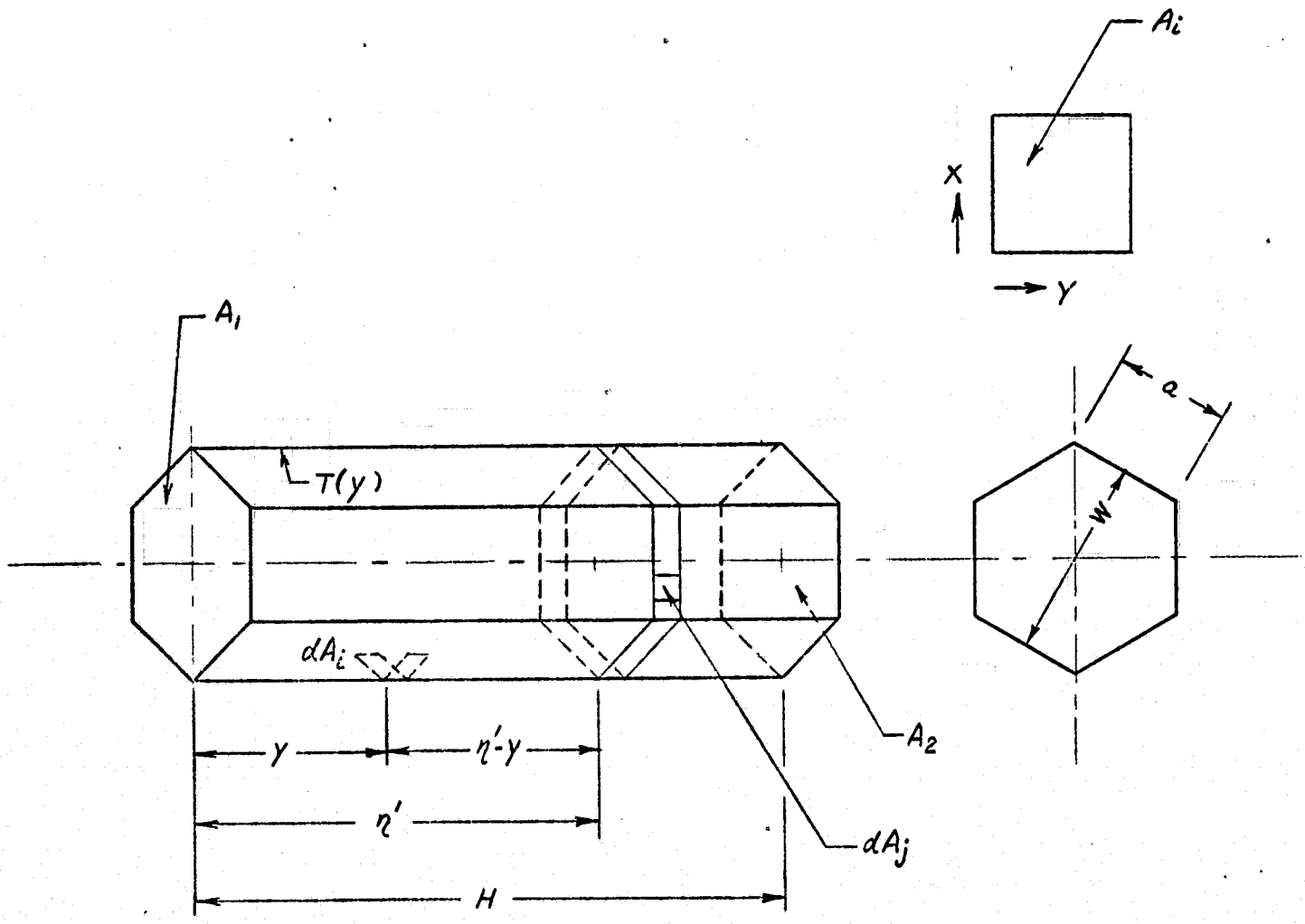

Figure 2. Single Isolated Honeycomb Cell

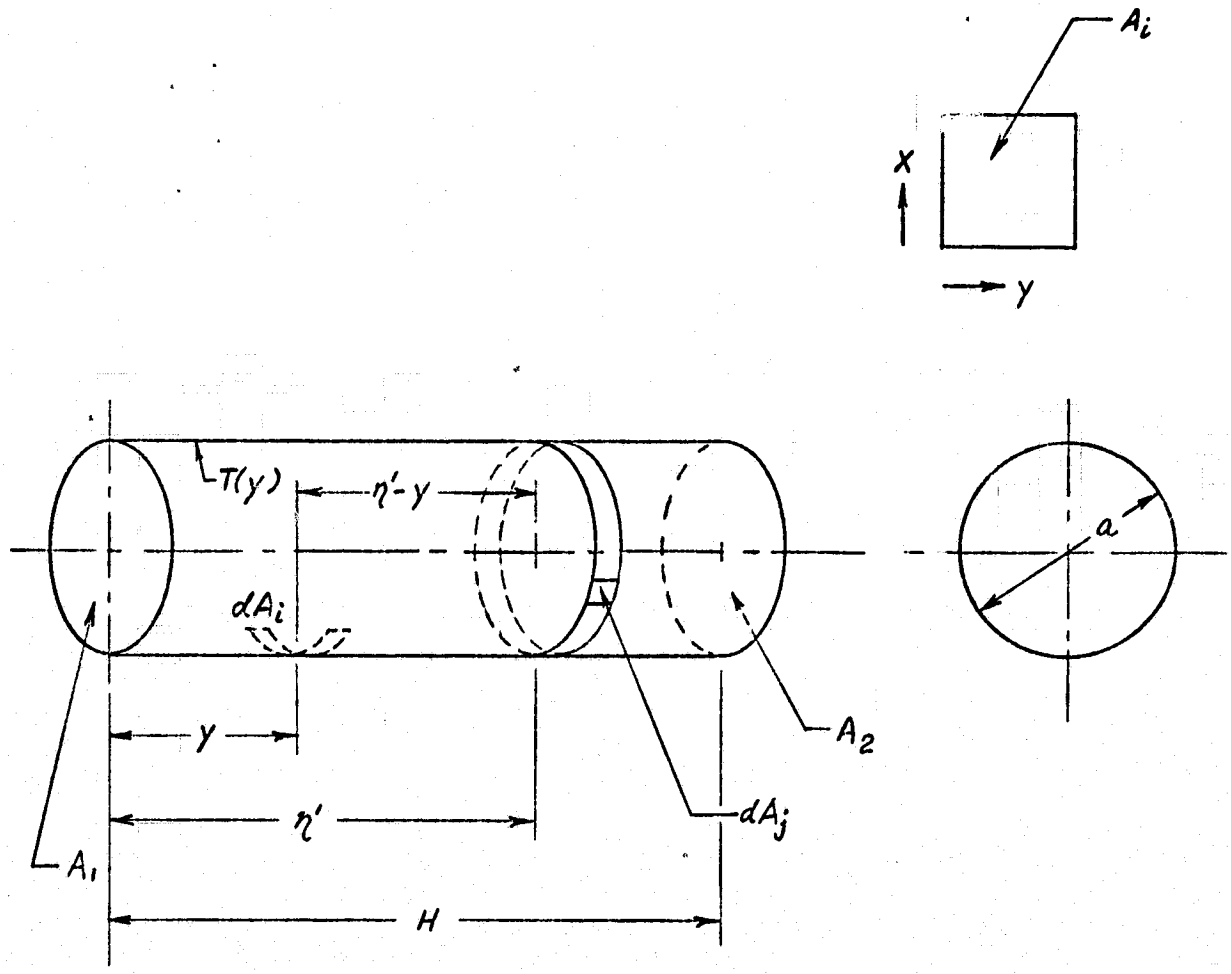

Figure 3. Hollow Cylindrical Enclosure

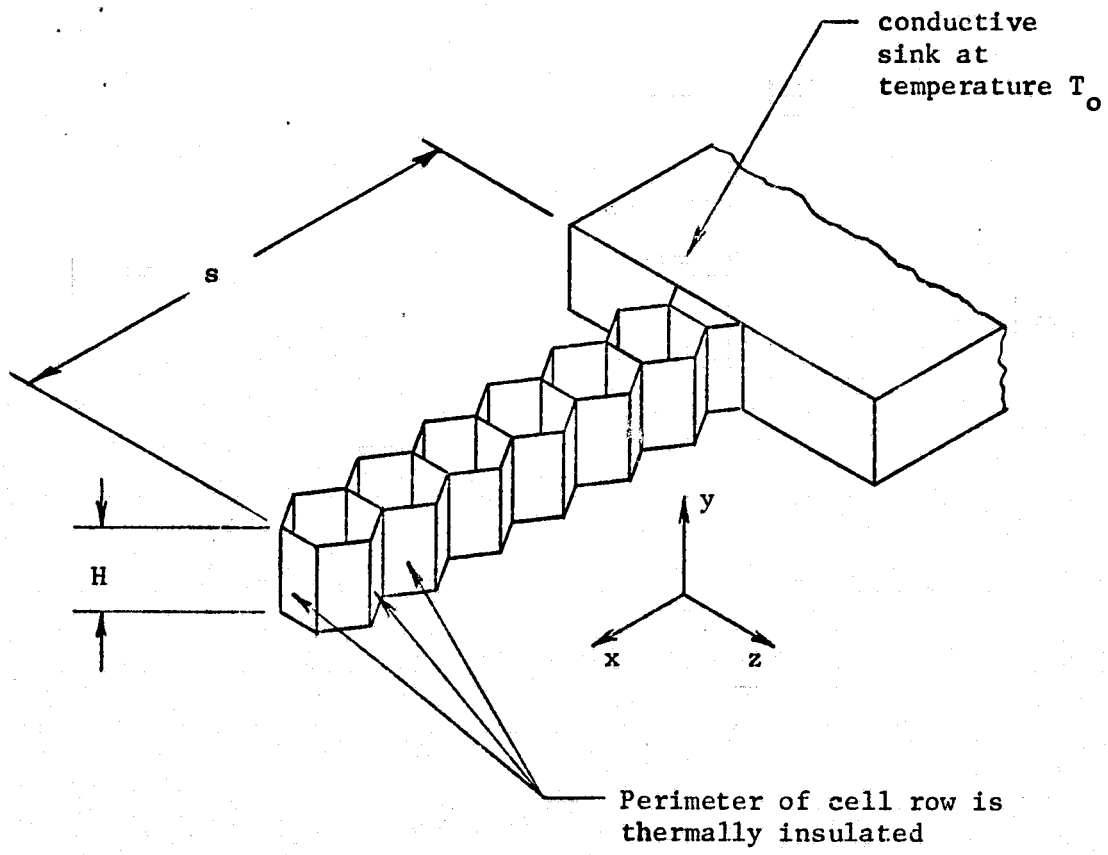

Figure 4. Isolated Cell Row, High Conductance Direction

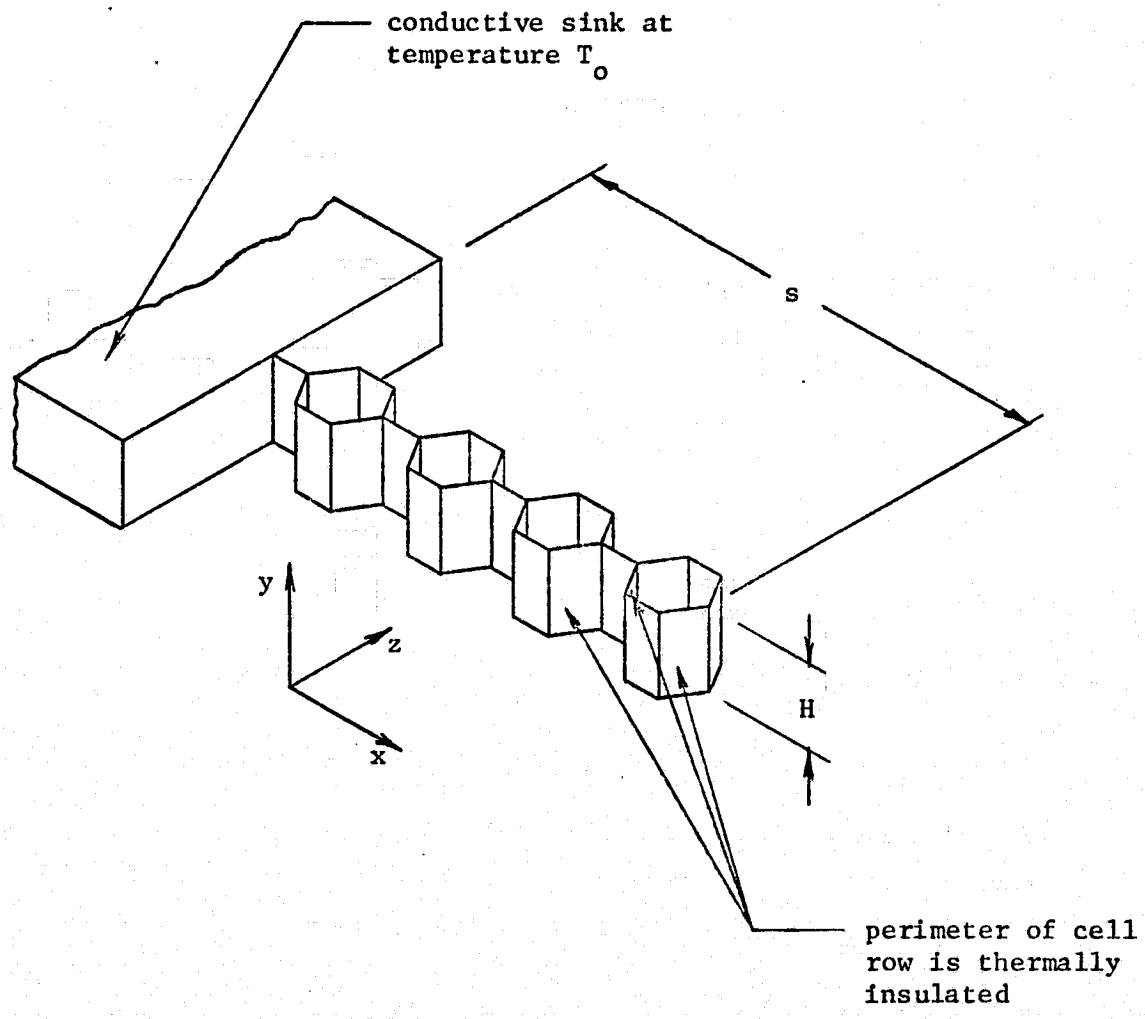

Figure 5. Isolated Cell Row, Low Conductance Direction

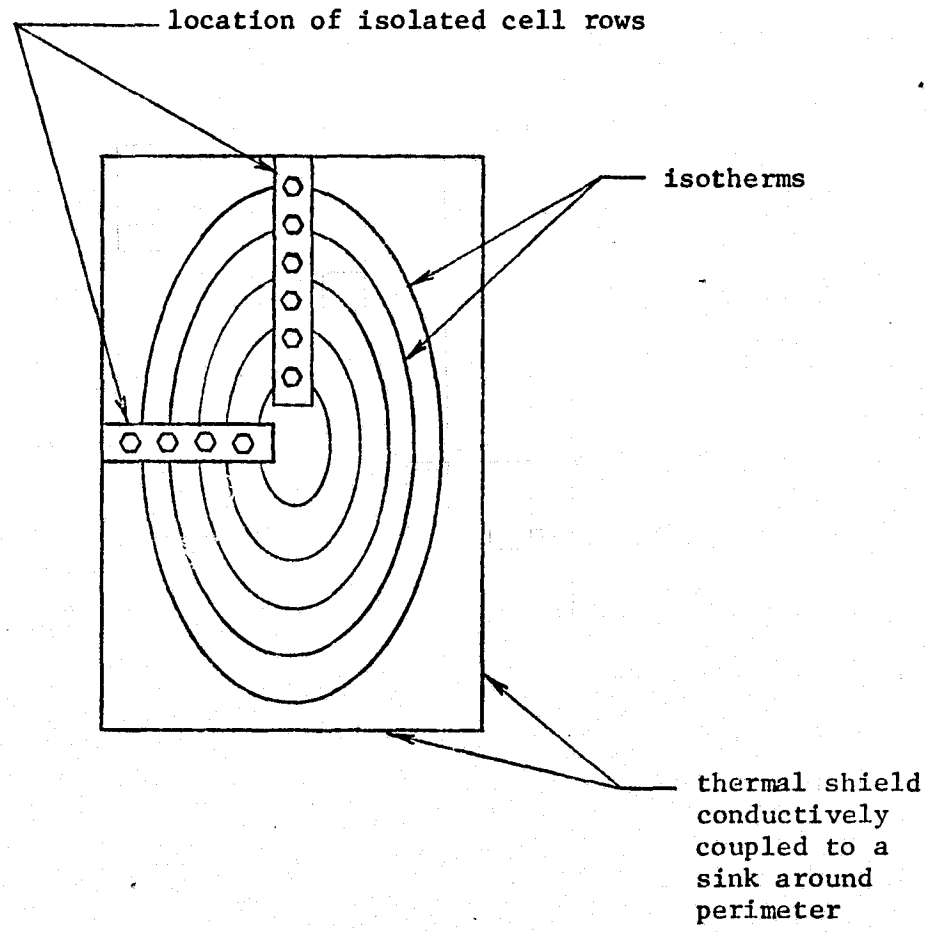

Figure 6. Location of Isolated Cell Rows in a Typical Honeycomb Thermal Shield

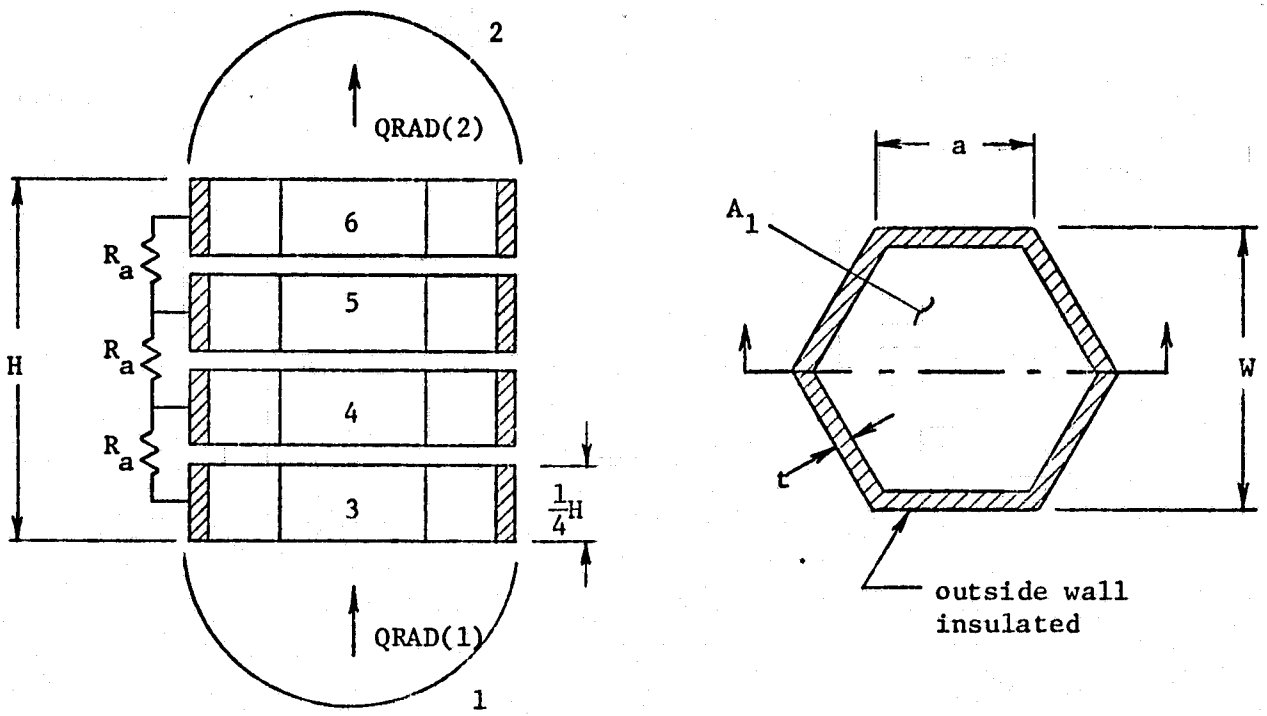

NODE NO.	DESCRIPTION
1	radiative source
2	radiative sink
3 thru 6	honeycomb elements

NOTES:

1. All nodes radiatively coupled
2. Nodes 3 thru 6 conductively coupled, diffuse surfaces
3. Nodes 1 and 2 diffuse, black sources
4. Energy transfer by radiation and conduction only

Figure 7. Single Cell Finite Element Model

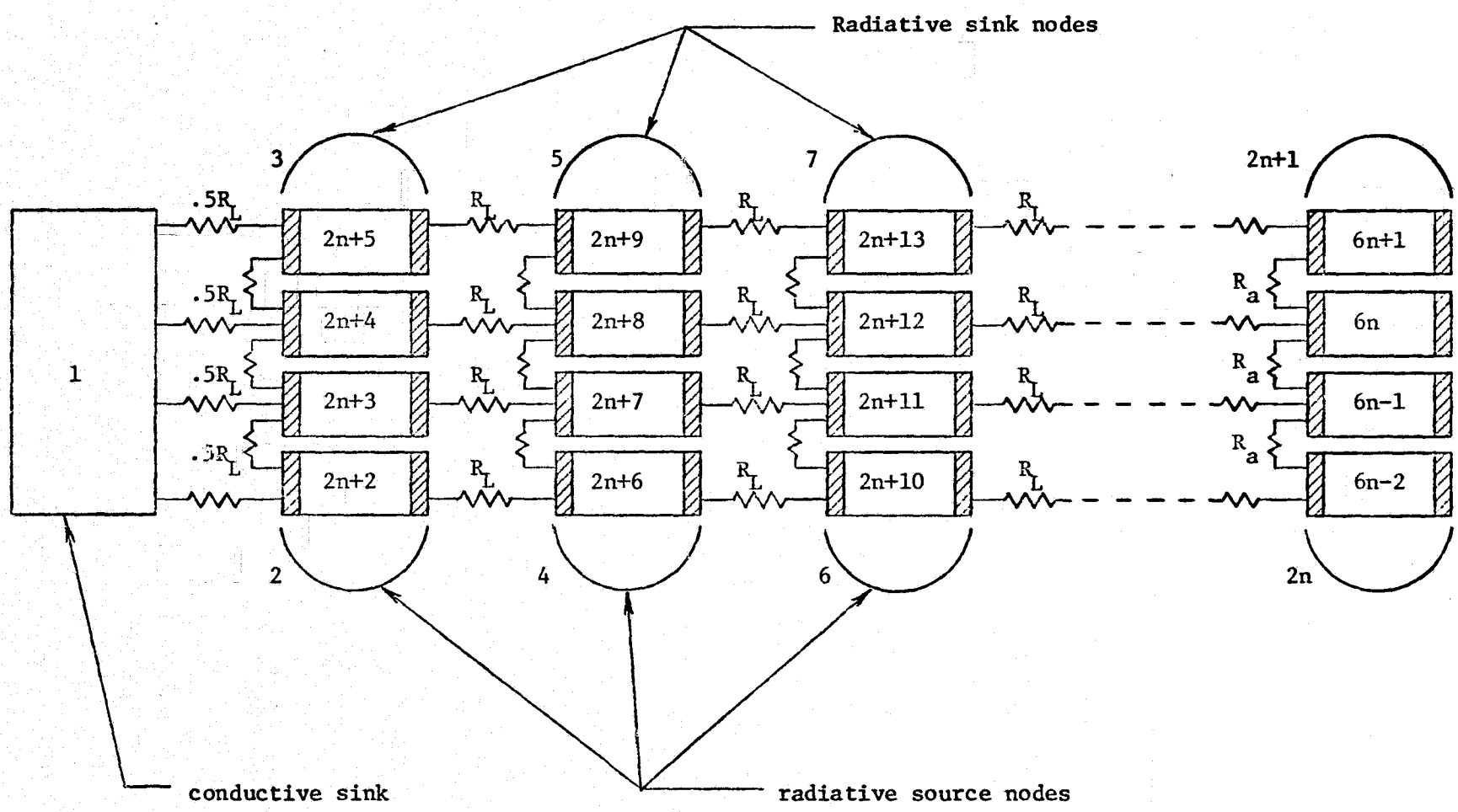

NOTES:
1. No radiative coupling between cells
2. Radiation resistance paths not shown
3. R_L is lateral conductive resistance
4. R_a is axial conductive resistance

Figure 8. Isolated Row Finite Element Model

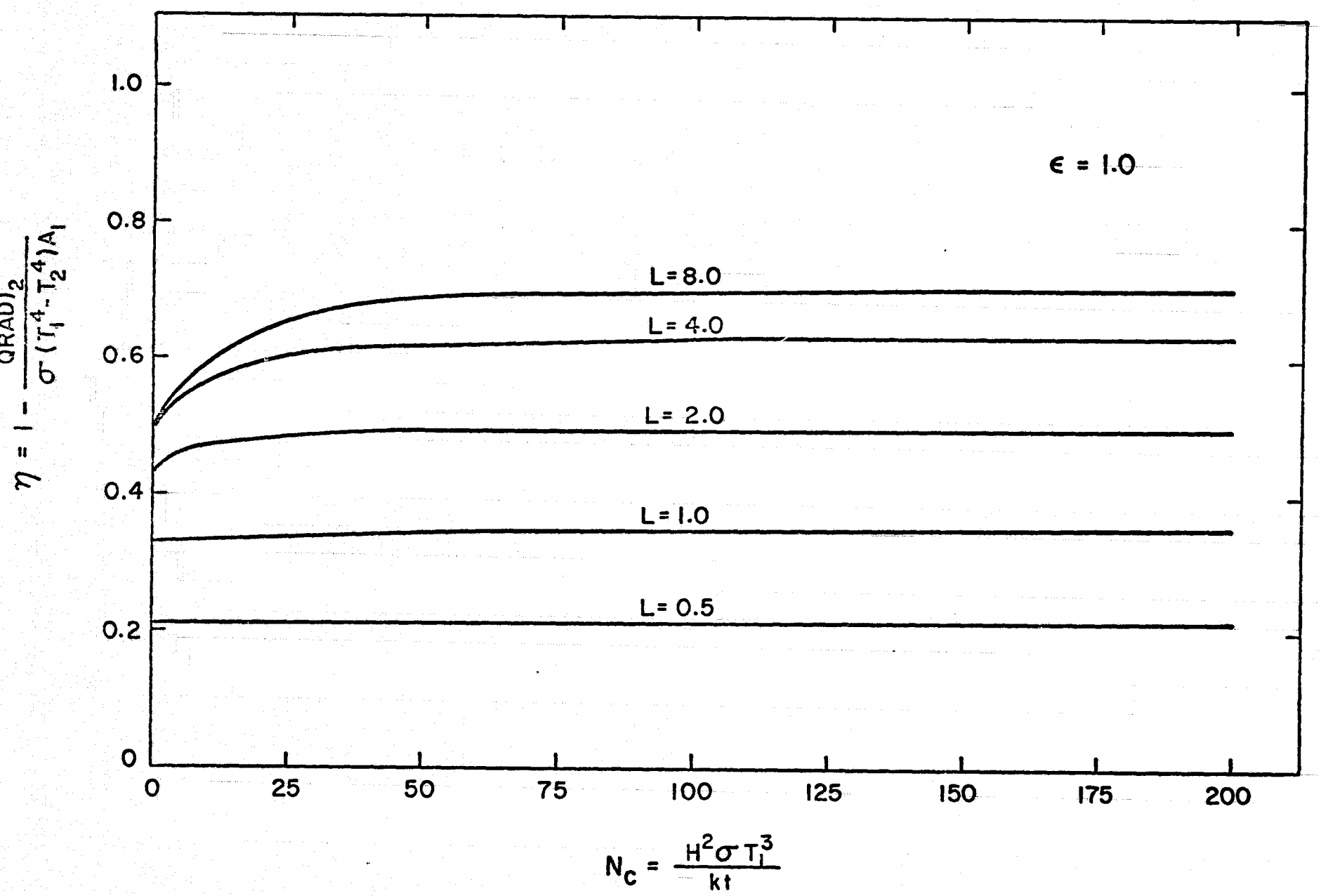

Figure 9. Efficiency vs N_c for Isolated Cells with $\varepsilon = 1.0$

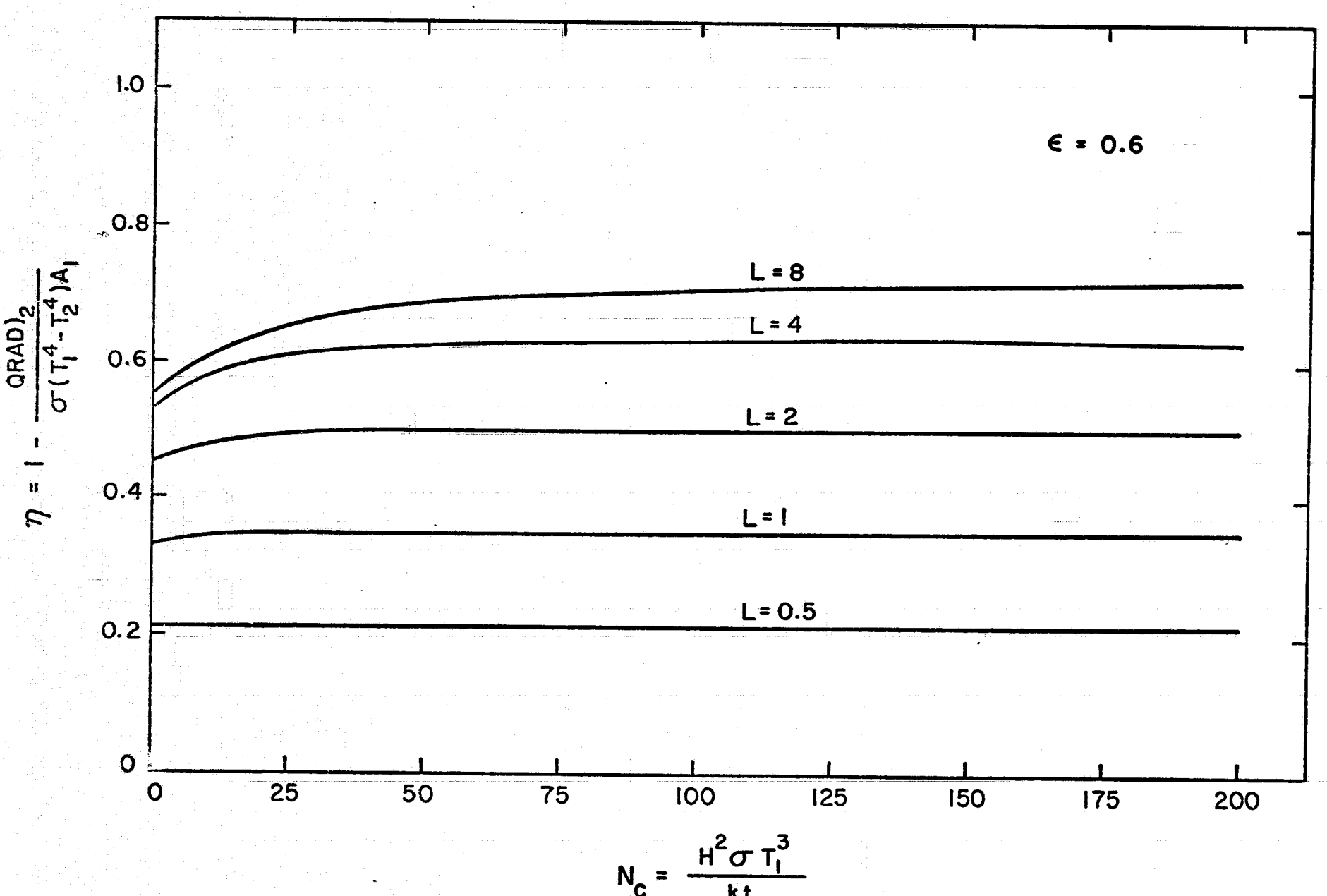

Figure 10. Efficiency vs N_c for Isolated Cells with $\varepsilon = 0.6$

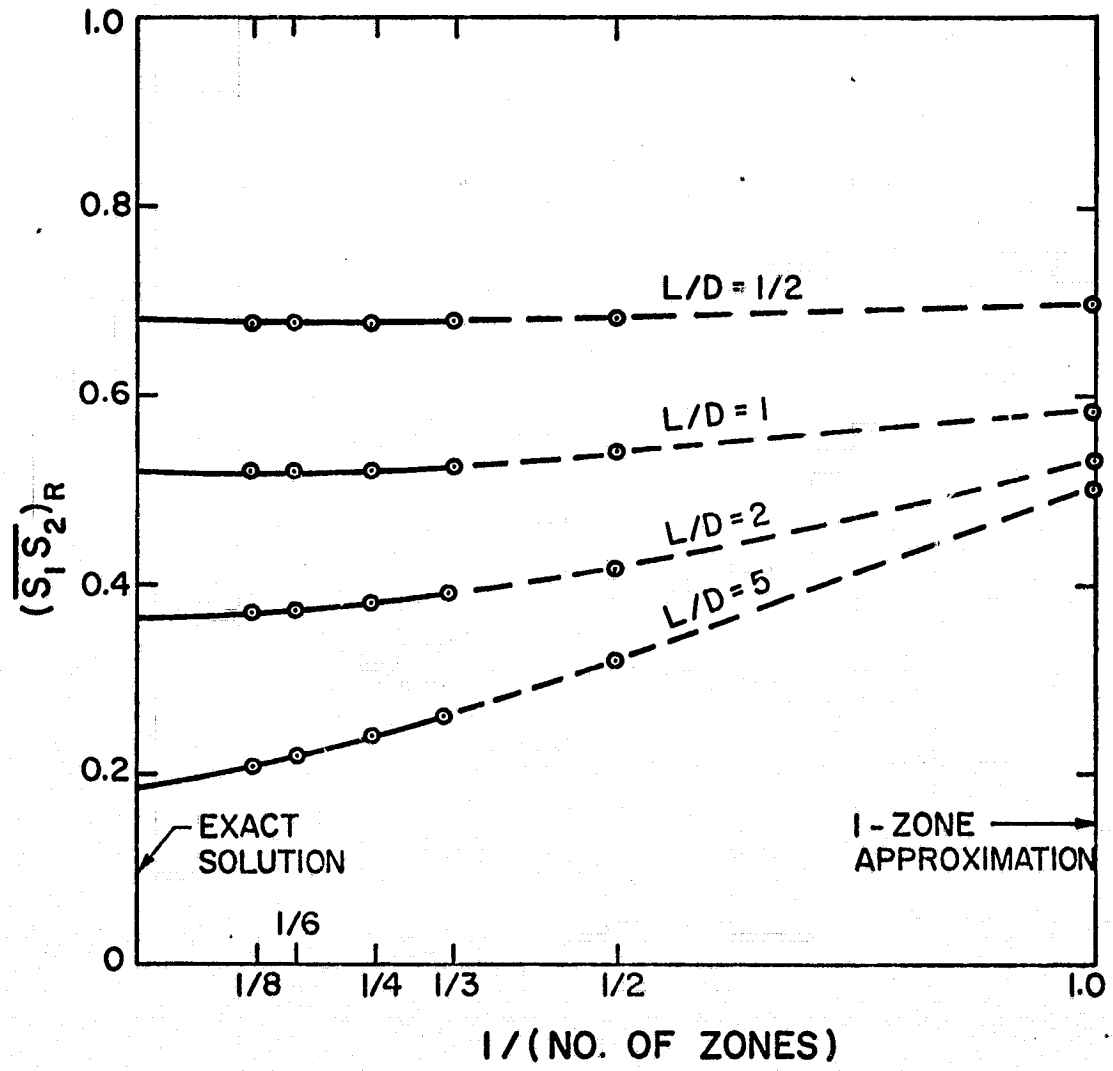

Figure 11. Efficiency, $[1 - (\overline{s_1 s_2})]$, vs number of honeycomb zones. Reproduced from Reference 1.

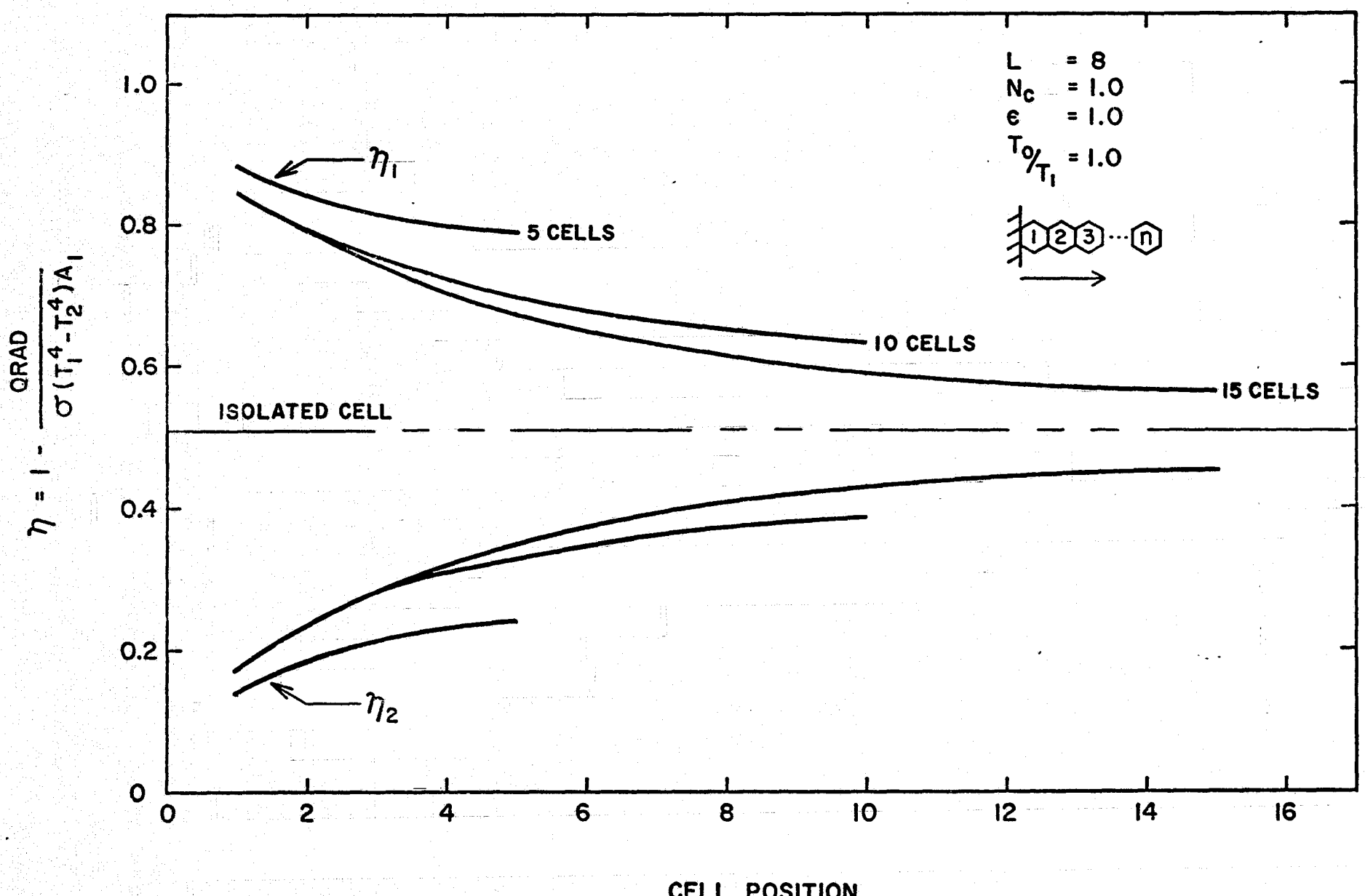

Figure 12. Efficiency vs Cell Position and Number of Cells per Row for L = 8.

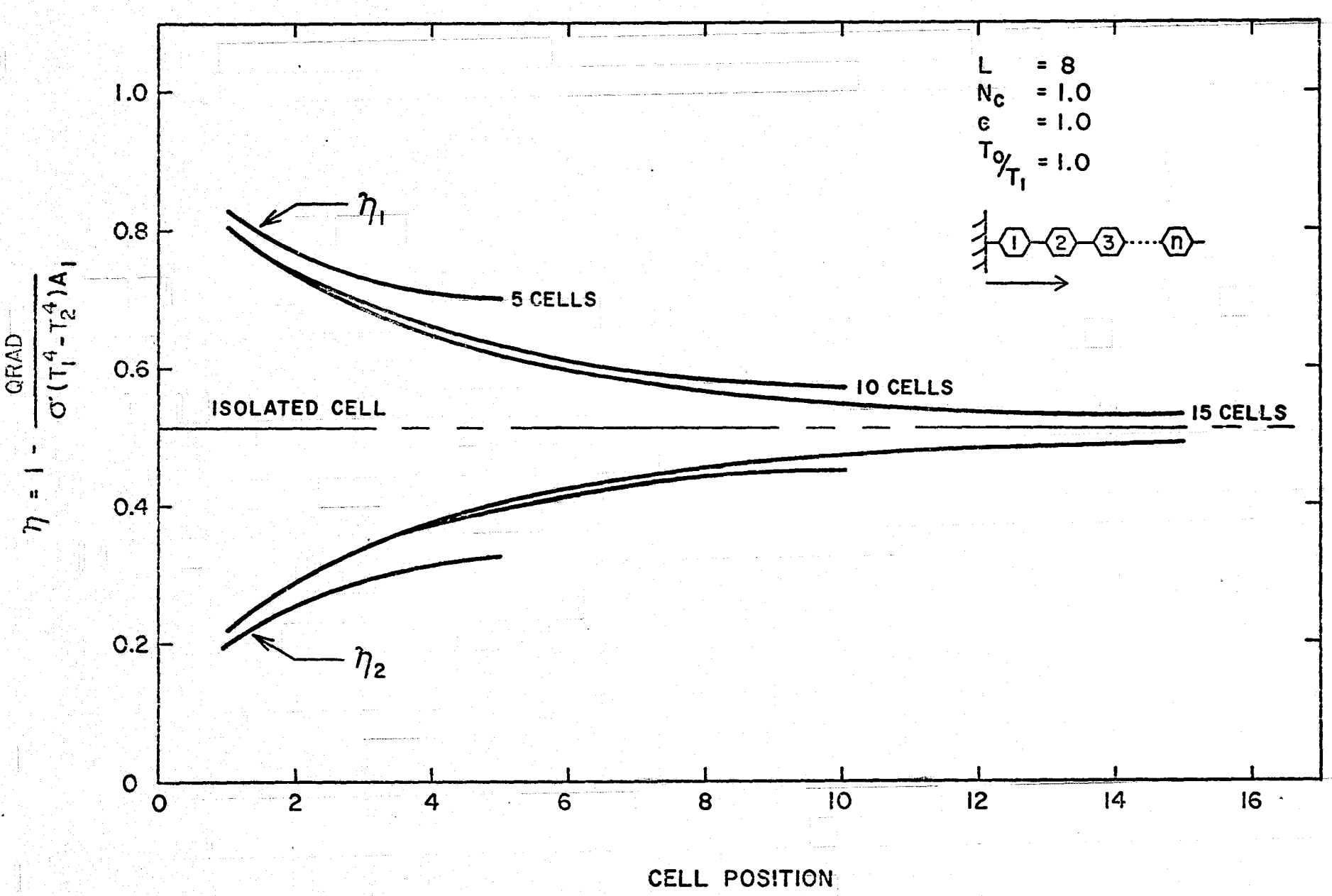

Figure 13. Efficiency vs Cell Position and Number of Cells per Row for L = 8.

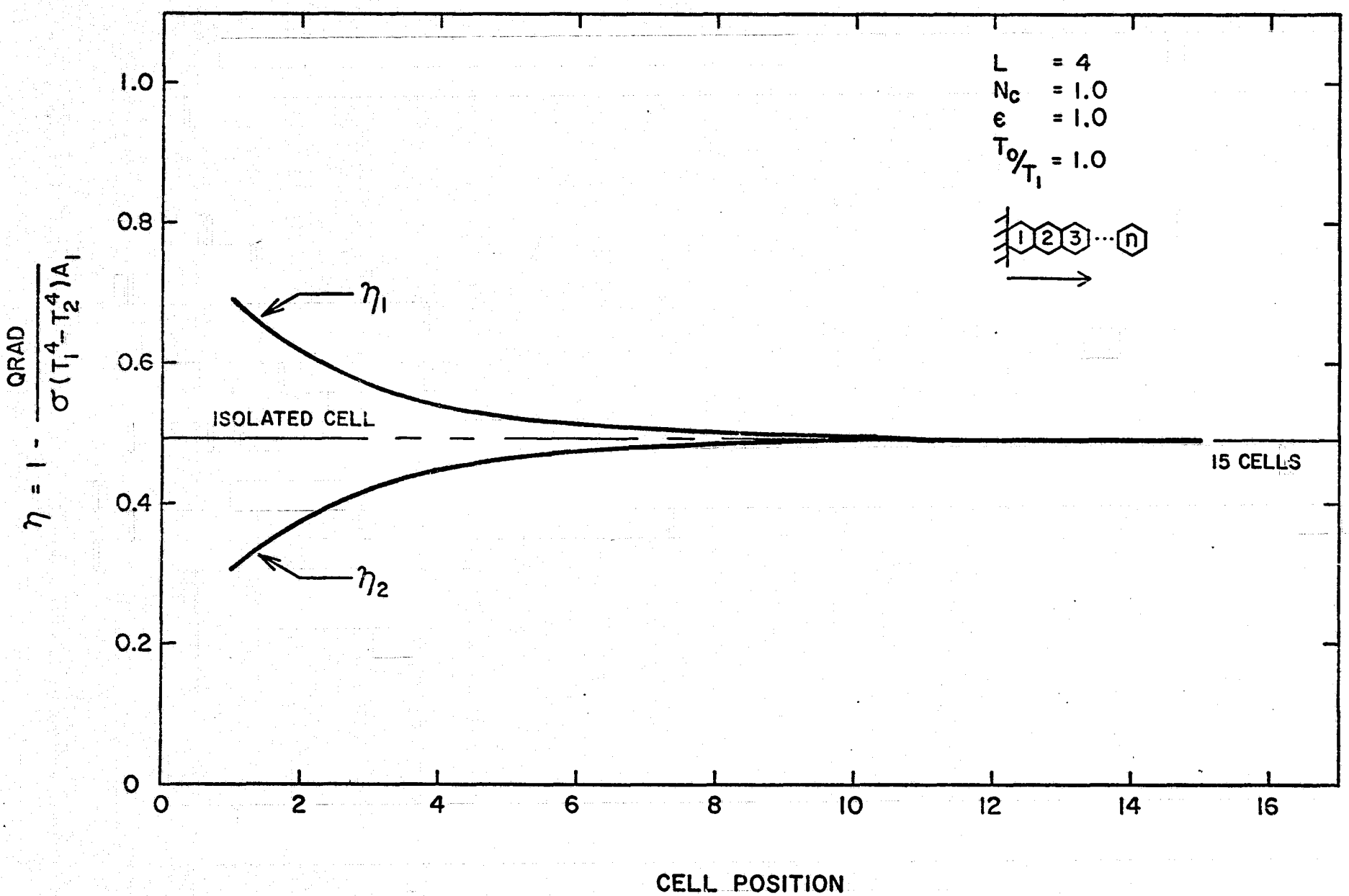

Figure 14. Efficiency vs Cell Position and Number of Cells per Row for L = 4.

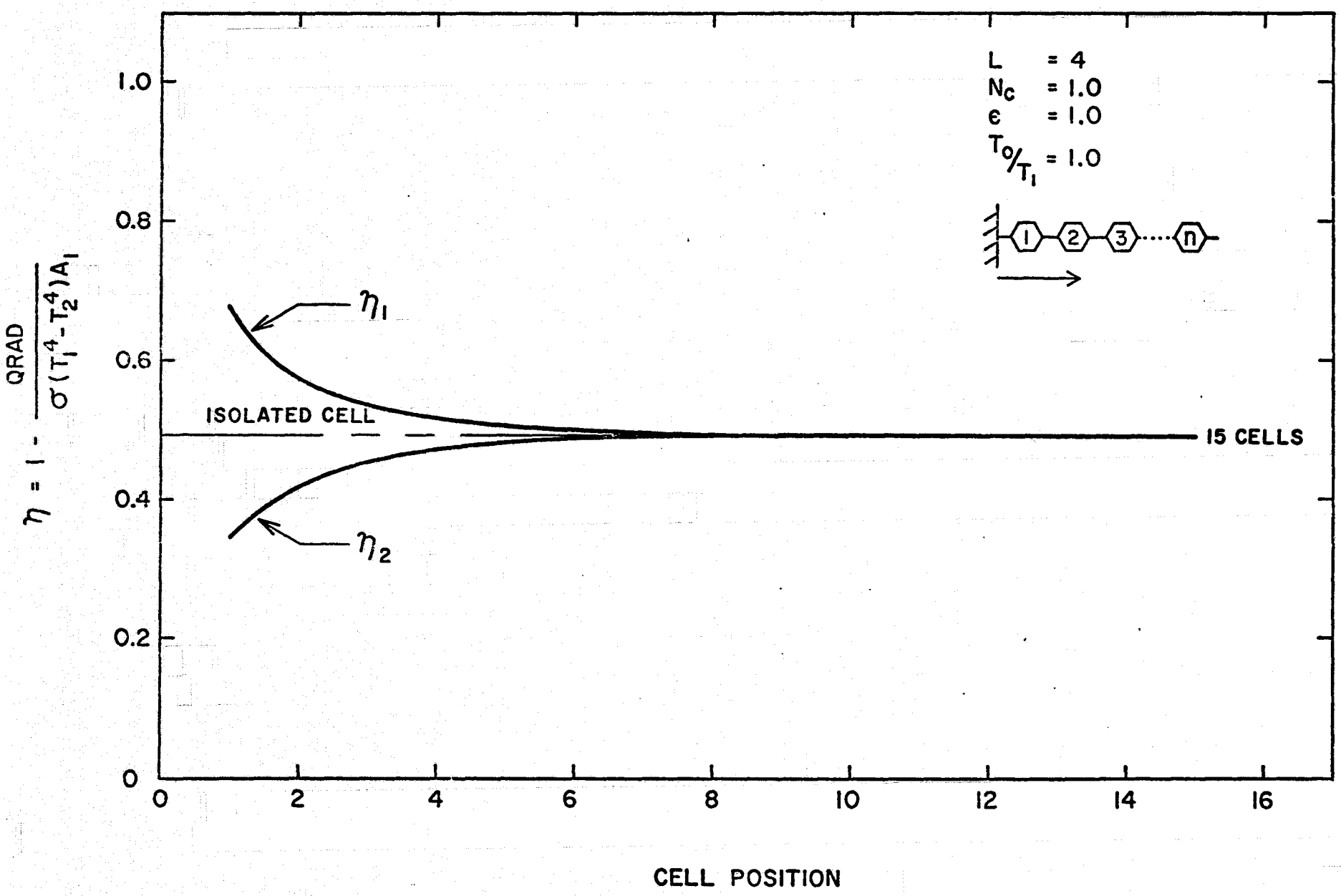

Figure 15. Efficiency vs Cell Position and Number of Cells per Row for L = 4.

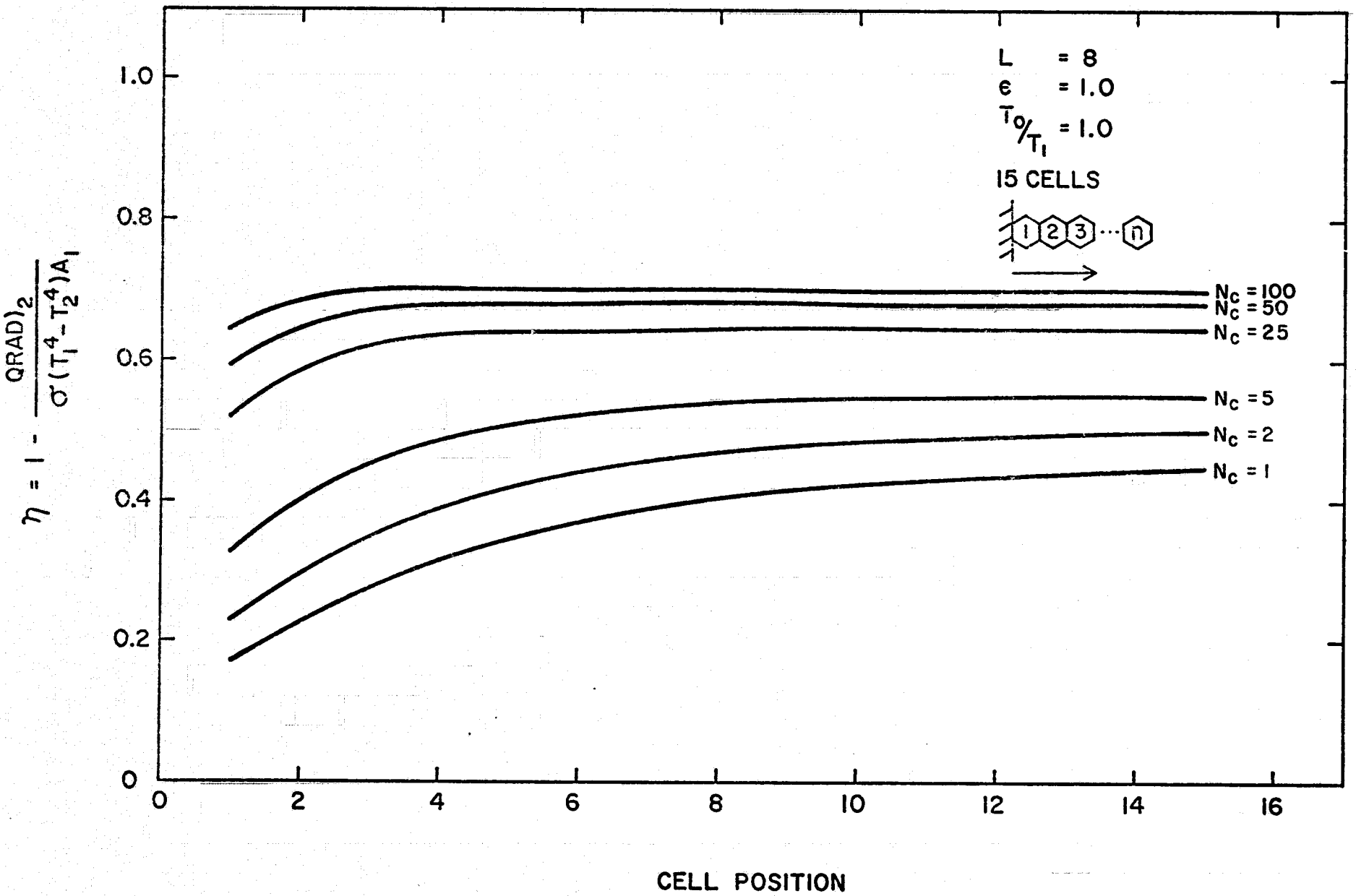

Figure 16. Efficiency vs cell position and N_c for L = 8.

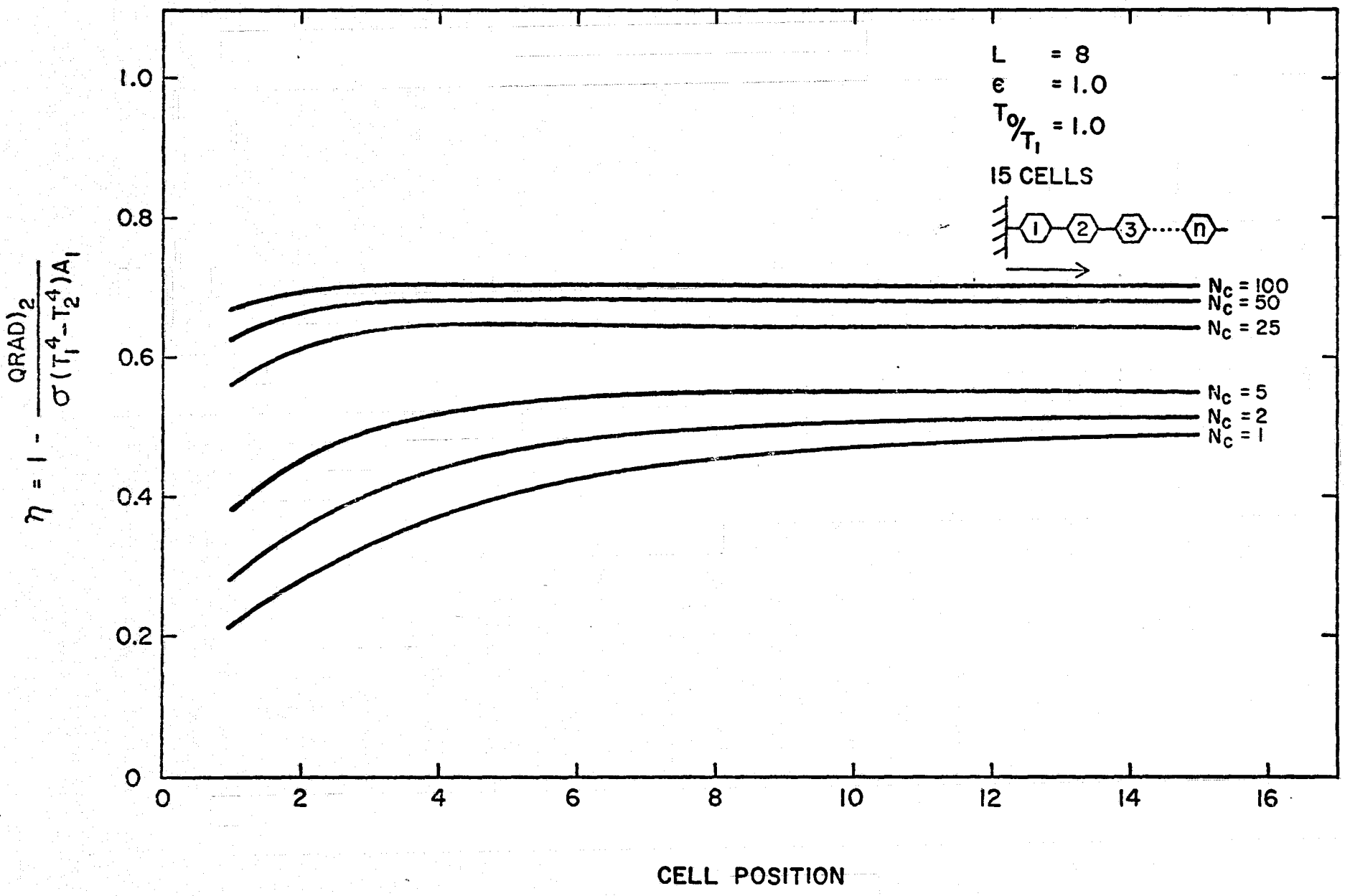

Figure 17. Efficiency vs cell position and N_c for L = 8.

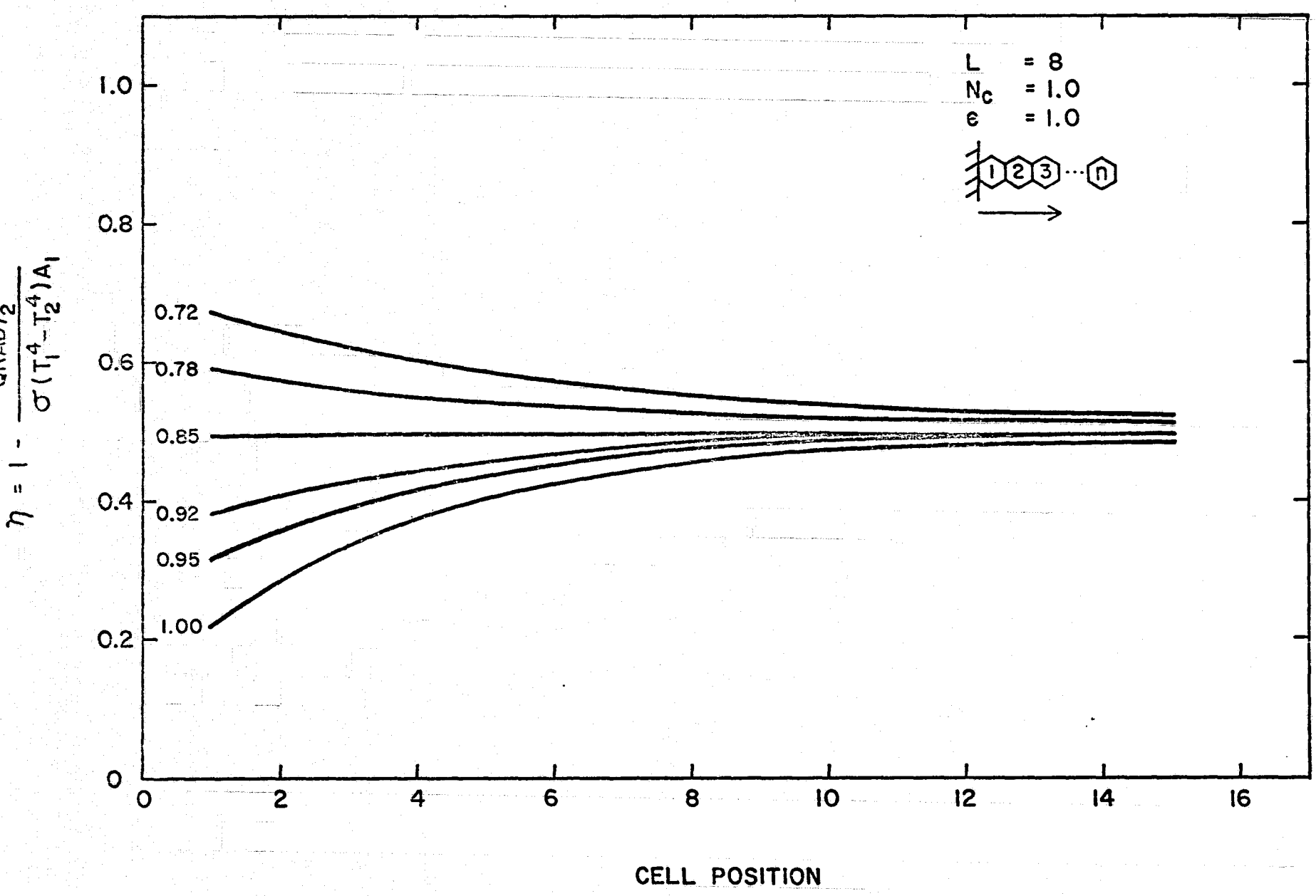

Figure 18. Efficiency vs cell position and (T_o/T_1) for L = 8.

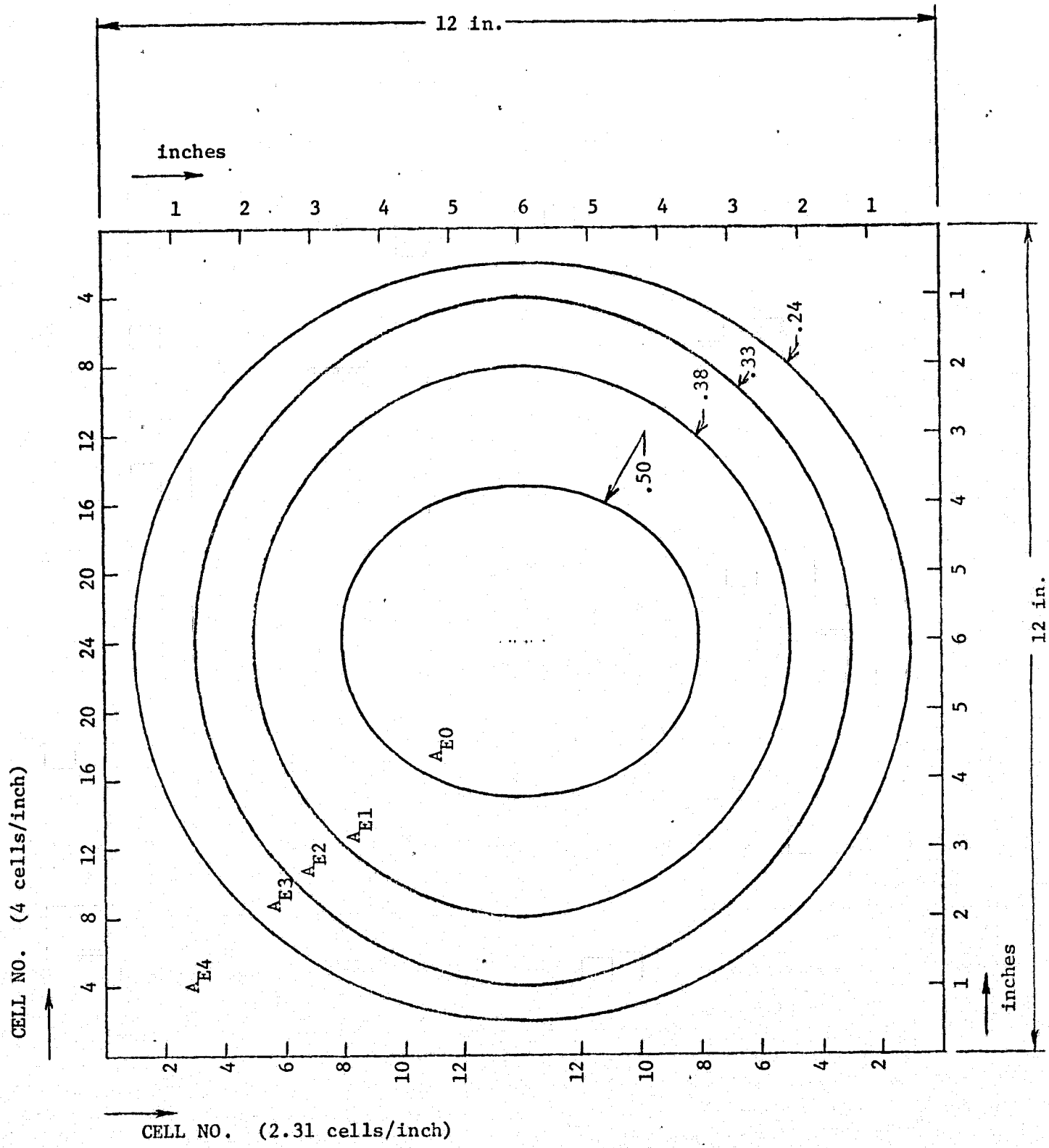

Figure 19. Lines of Equal Efficiency for Design Example Two.

APPENDIX C

REFERENCES AND RELATED PUBLICATIONS

1. Hottel, H. C. and A. F. Sarofim. Radiative Transfer. McGraw Hill, pages 37-39 and pages 106-112.

2. Usiskin, C. M. and R. Siegel, 1960: Thermal Radiation from a Cylindrical Enclosure with Specified Wall Heat Flux. Journal of Heat Transfer, Nov., p. 369.

3. Feingold, A., 1966: Radiant Interchange Configuration Factors Between Various Selected Plane Surfaces. Proc. Royal Society of London, May 3, pp. 51-60.

4. Sparrow, E. M. and R. D. Cess, Radiation Heat Transfer. Brooks/Cole Publishing Co., Chapters 3, 6.

5. Sparrow, E. M., 1961: The Effectiveness of Radiating Fins with Mutual Irradiation. Journal of Aerospace Sciences, Oct., p. 763.

6. Sparrow, E. M., 1962: Radiating Effectiveness of Annular-Finned Space Radiators, Including Mutual Irradiation Between Radiator Elements. Journal of Aerospace Sciences, Nov. p. 1291.

7. Treuenfels, E. W., 1963: Emissivity of Isothermal Cavities. Journal Optical Soc. of America, Oct. p. 1162.

8. Buckley, H., 1927: On the Radiation From the Inside of Circular Cylinder. Phil. Magazine, p. 753.

9. Leuenberger, H. and R. A. Pearson, 1956: Compilation of Radiation Shape Factors for Cylindrical Assemblies. ASME PAPER 56-A-144(1956).

10. Sparrow, E. M., 1962: Thermal Radiation Characteristics of Cylindrical Enclosures. Journal of Heat Transfer, Feb., p. 73.

11. Sparrow, E. M., 1965: Radiant Interchange Among Curved Specularly Reflecting Surfaces--Application to Cylindrical and Conical Cavities. Journal of Heat Transfer, May, p. 299.

12. Sparrow, E. M., 1962: An Enclosure Theory for Radiative Exchange Between Specularly and Diffuse Reflecting Surfaces. Journal of Heat Transfer, Nov., p. 294.

13. Sparrow, E. M., 1963: Thermal Radiation Absorption in Rectangular-Groove Cavities. Journal of Applied Mechanics, June, p. 237.

14. Sparrow, E. M., 1962: Radiant Emission from a Parallel Walled Groove. Journal of Heat Transfer, Aug., p. 270.

15. Sparrow, E. M., 1964: The Transport of Radiant Energy Through Tapered Tubes on Tapered Gaps. Journal of Heat Transfer, Feb., p. 132.

16. Perlmutter, M. and R. Siegel, 1963: Effect of Specularly Reflecting Gray Surfaces on Thermal Radiation Through a Tube and From Its Heated Wall. Journal of Heat Transfer, p. 55

17. Sparrow, E. M., 1963: Radiant Emission Characteristics of Diffuse Conical Cavities. Journal Optical Soc. of America, pp. 816-821.

18. Sparrow, E. M., 1971: Efficiencies of Honeycomb Absorbers of Solar Radiation. NASA TN-D-6337, May.

19. Goodwin, M. W., 1965: Conduction of Heat in Light-weight Composite Honeycomb Structures. AD-475-482, Sept.

20. Roane, L. and R. R. Howell, 1969: Exploratory Study of Open-Face Honeycomb to Reduce Temperature of Hypersonic Aircraft Structure. NASA TN D-5278, July.

APPENDIX D

CLEAR VIEW CALCULATION

The equivalent field of view of a detector shielded by a Honeycomb Thermal Shield can be approximated by:

$$\Omega_{eqv} = \Omega_{detector} - \frac{\pi}{6}\frac{\theta_D^{\,3}}{\theta_s}$$

where:

$$\Omega_{detector} = \pi\left(\frac{W}{g + H}\right)^2 = \text{solid angle in steradians}$$

$$g = [W^2 + H^2]^{1/2}$$

$$\theta_D = \tan^{-1}\left(\frac{W}{H}\right) \text{ for the detector collimator}$$

$$\theta_s = \tan^{-1}\left(\frac{W}{H}\right) \text{ for the Honeycomb Thermal Shield}$$

APPENDIX E

ANGLE FACTOR CALCULATION

For two cell areas, determine F_{4-5} if F_{1-2}, F_{1-3}, and F_{2-3} are known.

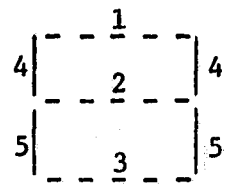

Honeycomb cell cross section

$$F_{4-5} = 1 - F_{4-1} - F_{4-4} - F_{4-3} \qquad \text{EQ 1}$$

Calculate F_{1-4}:

$$F_{1-4} = 1 - F_{1-2}$$

$$A_1F_{1-4} = A_4F_{4-1}$$

Then

$$F_{4-1} = \left(\frac{A_1}{A_4}\right)F_{1-4} = \left(\frac{A_1}{A_4}\right)[1 - F_{1-2}] \qquad \text{EQ 2}$$

Calculate F_{4-4}:

$$F_{4-4} = 1 - F_{4-1} - F_{4-2}$$

but $F_{4-1} = F_{4-2}$

then

$$F_{4-4} = 1 - 2F_{4-1} = 1 - 2\left(\frac{A_1}{A_4}\right)[1 - F_{1-2}] \qquad \text{EQ 3}$$

Calculate F_{4-3}:

$$F_{3-4} = F_{3-2} - F_{3-1}$$

$$A_3F_{3-4} = A_4F_{4-3}$$

$$F_{4-3} = \left(\frac{A_3}{A_4}\right)F_{3-4} = \left(\frac{A_3}{A_4}\right)[F_{3-2} - F_{3-1}] \qquad \text{EQ 4}$$

Combining Equations 1 through 4:

$$\boxed{F_{4-5} = \left(\frac{A_1}{A_4}\right)[1 - 2F_{1-2} + F_{1-3}]}$$

The configuration factor between two neighboring cell elements is easily expressed in terms of values appearing in Table E1.

Continuing the procedure to determine the factors for cell elements separated by a third element:

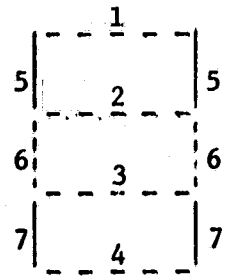

$$F_{5-7} = \left(\frac{A_1}{A_5}\right)[F_{1-2} - 2F_{1-3} + F_{1-4}]$$

Finally, for a separation of two elements:

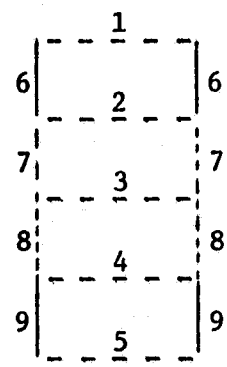

$$F_{6-9} = \left(\frac{A_1}{A_6}\right)[F_{1-3} - 2F_{1-4} + F_{1-5}]$$

The values of F_{1-2} used in Equation 1 are tabulated in Reference 3 and listed below:

$(\frac{1}{L})$	F_{1-2}
0.05	0.002056
0.10	0.008134
0.20	0.031042
0.30	0.065003
0.40	0.105661
0.50	0.149277
0.60	0.193186
0.70	0.235742
0.80	0.276046
0.90	0.313693
1.00	0.346850
1.50	0.485958
2.00	0.578372
2.50	0.643424
3.00	0.691350
4.00	0.756932
5.00	0.799577

$(\frac{l}{L})$	F_{1-2}
6.00	0.829491
7.00	0.851625
8.00	0.868664
9.00	0.882186
10.00	0.893177
11.00	0.902289
12.00	0.909965
13.00	0.916521
14.00	0.922184
15.00	0.927126
16.00	0.931476
17.00	0.935336
18.00	0.938783
19.00	0.941880
20.00	0.944679

Configuration factor between base elements of a honeycomb cell (Reference 3).

TABLE E1